Composition of pumpellyite, epidote and chlorite from New Caledonia : how important are metamorphic grade and whole-rock compositon?

Autor(en): **Potel, Sébastien / Schmidt, Susanne Th. / Capitani, Christian de**

Objekttyp: **Article**

Zeitschrift: **Schweizerische mineralogische und petrographische Mitteilungen = Bulletin suisse de minéralogie et pétrographie**

Band (Jahr): **82 (2002)**

Heft 2: **Diagenesis and Low-Grade Metamorphism**

PDF erstellt am: **26.09.2024**

Persistenter Link: https://doi.org/10.5169/seals-62363

SCHWEIZ. MINERAL. PETROGR. MITT. 82, 229–252, 2002

Composition of pumpellyite, epidote and chlorite from New Caledonia – How important are metamorphic grade and whole-rock composition?

by *Sébastien Potel*[1*], *Susanne Th. Schmidt*[2] and *Christian de Capitani*[1]

Abstract

In New Caledonia, pumpellyite occurs in association with epidote, chlorite and amphibole in metabasites, metapelites and metatuffs. The metamorphism in New Caledonia is related to two subduction events, one during Cretaceous time and a second one during Oligocene time. Metamorphism in the different metamorphic zones displays an increase in metamorphic grade from pumpellyite-actinolite (Pmp-Act) facies at high pressure to prehnite-pumpellyite (Prh-Pmp) facies at intermediate to low pressure.

Detailed chemical analysis of pumpellyite, epidote, chlorite and actinolite from various lithologies shows different compositions in the metamorphic zones. Bulk-rock compositions, metamorphic grade and mineral associations were determined to define the factors that control these mineral compositions.

Equilibrium phase diagrams were calculated using the DOMINO-THERIAK software and an updated thermodynamic database. To test the effect of bulk-rock composition, the calculations were done in systems of varying Mg/(Mg+Fe) and Al/(Fe+Al) ratios at 3 kbar and using the hematite-magnetite buffer as a control for aO_2. Equilibrium assemblages corresponding to observed mineral associations occur in the predicted phase diagrams. Pumpellyite is stable over a wide compositional range in these different systems at temperatures below 235 °C, whereas epidote becomes stable at temperatures above 235 °C. In systems of low Mg/(Mg+Fe) and high Al/(Fe+Al), epidote and pumpellyite are predicted to be stable between 235 and 290 °C. The association pumpellyite-prehnite appears to be characteristic of low Mg/(Mg+Fe) and high Al/(Fe+Al), whereas the association pumpellyite-actinolite seems to be characteristic of high Mg/(Mg+Fe) systems. Variations of oxygen fugacity play an important role on the observed mineral associations and the compositions of pumpellyite and epidote.

Keywords: pumpellyite-prehnite facies, pumpellyite-actinolite facies, epidote, oxygen fugacity, equilibrium phase diagram.

Introduction

Since the pioneering work of HASHIMOTO (1966), several studies have been published on the composition of coexisting phases in rocks of very low- and low-grade metamorphism.

In low-grade metamorphic rocks, pumpellyite is an important index mineral found in basic rocks metamorphosed at various pressures and under low temperature conditions resulting in the prehnite-pumpellyite, the pumpellyite-actinolite and the blueschist facies. Therefore, pumpellyite is diagnostic of two of the principal facies of low-grade metamorphism. For this reason, the variation of its chemical composition as a possible indicator of metamorphic grade has been studied (for a review see BEIERSDORFER and DAY, 1995). For example, several authors have attempted to link variations in Al-Fe composition of pumpellyite with variations in metamorphic grade. Different tendencies are observed: either a decrease of total Fe in pumpellyite with increasing grade due to the Al-Fe^{3+} exchange (COOMBS et al., 1976; BEVINS, 1978; LIOU, 1979) or, alternatively, the high total Fe is considered to be characteristic of lower metamorphic grade (BEVINS, 1978; SCHIFFMAN and

[1] Mineralogisch-Petrographisches Institut der Universität Basel, Bernoullistrasse 30, CH-4056 Basel, Switzerland.
[2] Département de Minéralogie, Rue des Maraîchers 13, CH-1211 Geneva, Switzerland.
[*] Present address: Institut für Geowissenschaften, Senckenbergstrasse 3, D-35490 Giessen, Germany.
<sebastien.potel@geolo.uni-giessen.de>

LIOU, 1980). COOMBS et al. (1976), ISHIZUKA (1991) and others observed that Fe-rich pumpellyite occurs in the lowest-grade metamorphic zones, whereas aluminous varieties appear in the pumpellyite-actinolite and blueschist zones. In contrast, CORTESOGNO et al. (1984) found no relation between total Fe and metamorphic grade, but they proposed that the composition of the precursor minerals was an important factor for both total Fe and Fe/(Fe+Al) in pumpellyite. The whole-rock composition (BANNO, 1964) and fO_2 (LIOU, 1979) are also known to influence the composition of this mineral. AGUIRRE (1993) correlated the chemical composition of pumpellyite to a specific geological setting.

Attempts to interpret the composition of epidote in relation to metamorphic grade have also been made (for a review see BEIERSDORFER and DAY, 1995). $Fe^{3+}/(Fe^{3+}+Al)$ in epidote is considered to decrease with increasing metamorphic grade (BIRD et al., 1988, TERABAYASHI, 1988; AIGUIRRE et al., 1989) but the opposite trend is

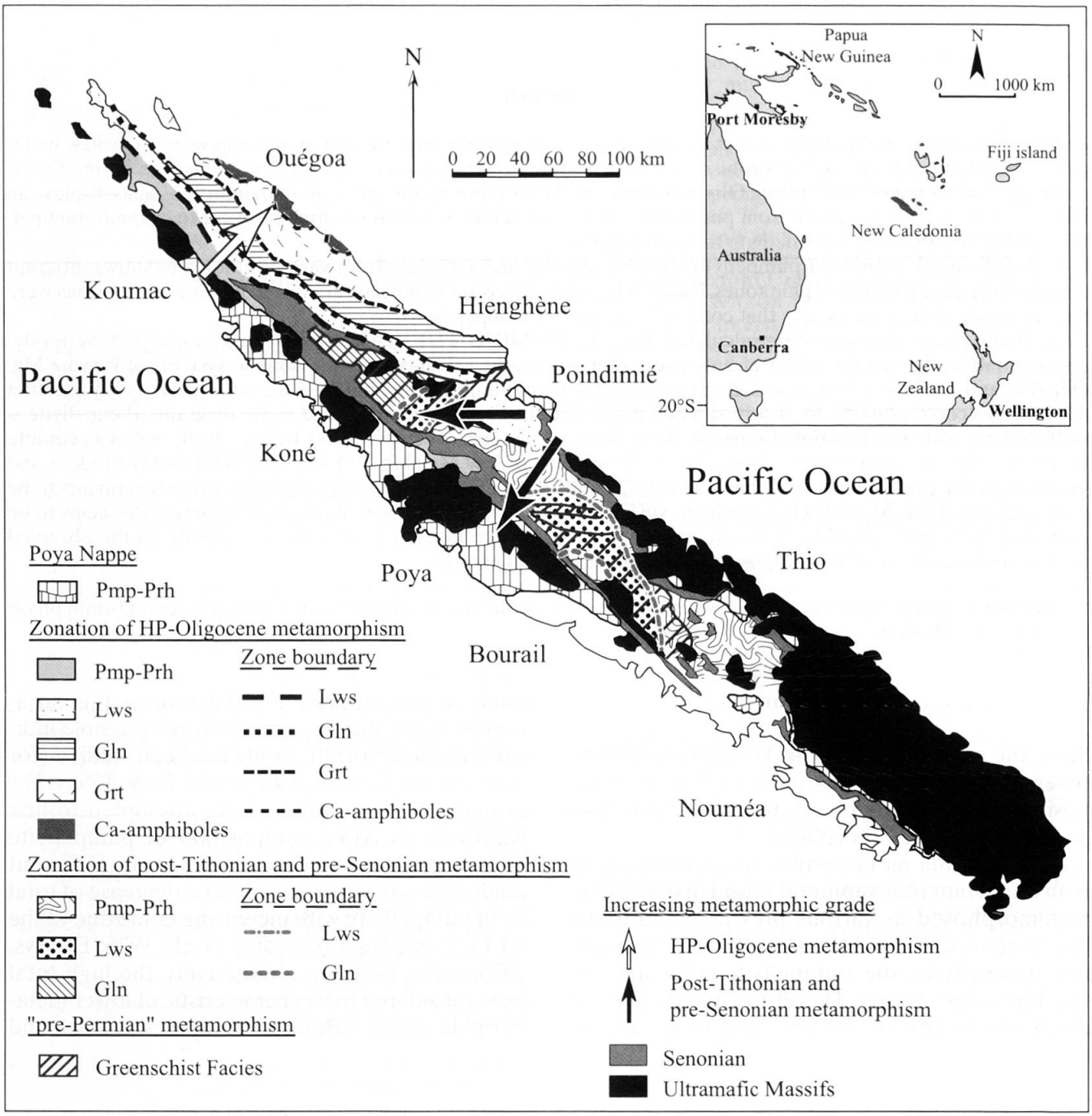

Fig. 1 Metamorphic map of New Caledonia after PARIS (1981). The arrows indicate two metamorphic field gradients. White arrow—increasing metamorphic direction of the Oligocene HP-metamorphism. Black arrows—increasing metamorphic grade of Cretaceous (post-Tithonian, pre-Senonian) metamorphism.

also reported (Levi et al., 1982; Cho et al., 1986). Liou (1973) observed that the maximum Fe^{3+} content of synthetic epidote varies as a function of fO_2, although Aiba (1982) found that epidote composition primarily depends on whole-rock composition.

Minerals of the chlorite group, mainly Fe-Mg-Al-chlorites, are among the most common phyllosilicates in metabasites and metapelites that form under low-temperature metamorphism. Numerous studies have been performed to determine which factors control the composition of chlorite in such rocks. Beiersdorfer and Day (1995) described five compositional parameters of chlorite, which can vary as a function of metamorphic grade: (1) Fe/(Fe+Mg), (2) Al/(Al+Fe), (3) tetrahedral Al, (4) octahedral vacancies, and (5) the proportion of swelling phyllosilicates.

Following previous studies on the composition of coexisting phases in very low- and low-grade metamorphic rocks, we present results of a comparison between naturally observed assemblages in New Caledonia and assemblages predicted by thermodynamic calculations. The island of New Caledonia offers the possibility to study a suite of metabasites and metapelites which contain pumpellyite, epidote and chlorite, and were metamorphosed under various grades. We examined mineral assemblages and their progressive evolution from prehnite-pumpellyite to pumpellyite-actinolite facies, to understand which parameters control the composition of pumpellyite, epidote and chlorite. Mineral assemblages and compositions of the relevant minerals were studied and compared to whole rock compositions. Analytical techniques included X-ray diffraction (XRD), electron microprobe (EMPA), and X-ray fluorescence (XRF). Because oxygen fugacity was considered by several authors (Liou, 1973; 1979) as a non-negligible factor, this has also been incorporated in our calculations. Equilibrium phase diagrams were calculated using the DOMINO-THERIAK software (de Capitani, 1994) in order to model the stable phase relations involving pumpellyite, epidote and chlorite as a function of temperature, whole rock composition, oxygen activity and pressure.

General geology

New Caledonia is a narrow and elongate island, some 400 km long and 40–50 km wide, located between latitudes 18° S and 22° S, roughly midway between Australia and the Fiji Islands and between New Zealand and New Guinea (inset of Fig. 1). The microcontinent of New Caledonia contains different terranes, which formed in different settings during the Permian to Oligocene. During the Late Palaeozoic–Mesozoic New Caledonia belonged to the Gondwana continent and was affected by subduction and accretion (Aitchison et al., 1998). Rifting-passive margin development and the formation of the New Caledonian block (NCB) resulted from the break-up of the Gondwana margin (Gaina et al., 1998). During late Cretaceous–Palaeocene time, two separate and distinct oceanic nappes, the Poya and Peridotite nappes, were obducted NE–SW onto the NCB (Eissen et al., 1998). Unroofing of the metamorphic core complexes was caused by late-stage gravitational collapse of the obducted ophiolite pile (Aitchison et al., 1995).

Petrographic descriptions

In New Caledonia, metabasic rocks occur in three areas: (1) In the high pressure (HP) metamorphic zone (Fig. 1), metabasic rocks are interbedded with metapelites (Espirat and Millon, 1965). This zone corresponds to the Oligocene metamorphic zone. (2) In the Poya nappe, which is composed of pillow basalts and includes pelagic sediments (shales and black cherts), dolerites and gabbros. This nappe represents the upper part of a slice of oceanic crust. (3) In the Cretaceous metamorphic zone where tuffs of Triassic–Jurassic age and basalts of doleritic composition are dominant. Metabasites are also interbedded with sediments and consist of volcanic rocks (dolerites) and tuffs. Samples for the present study were collected in the HP metamorphic zone, the Poya nappe and in the Cretaceous metamorphic zone, and are listed in Table 1, which also summarizes the observed mineral assemblages.

Basalts and dolerites in all zones are massive dark rocks (black to green), often with veins of epidote, quartz or sulphide. Thin sections show quartz, chlorite, epidote, pumpellyite, prehnite and an overgrowth assemblage, with green hornblende and actinolite mainly replacing clinopyroxene. These minerals grow on igneous precursors, but also in veinlets. The texture is medium-grained and relic phenocrysts of oligoclase are replaced by sericite, pumpellyite or prehnite. New growth of Na-amphibole, actinolite and chlorite is observed along the rims of magmatic hornblende. Tuffs are composed of fine-grained mica, chlorite and albite. In addition to the main assemblage, lawsonite, pumpellyite, epidote and Fe-stilpnomelane are found in all three metamorphic zones; the grades range from prehnite-pumpellyite to pumpellyite-actinolite facies.

Table 1 Mineral assemblages in basic rocks, metapelites and one tuff.

Samples	Rock type	Latitude	Longitude	Alt. (m)	Metamorphic assemblages (Ab+Mag+Qtz±Ttn±sulfides)	Relic phases	Accessory minerals	Facies
HP-Oligocene metamorphic zone								
MF3022	basalt	20°25'39"	164°23'06"	120	Chl-Ms-Act-Ep	Aug	Hem	Lws-Ab-Chl
MF3023	basalt	20°25'39"	164°23'12"	120	Chl-Lws, Chl-Act-Ep	Mg-Hb	Hem, Ap	Lws-Ab-Chl
MF3047	syeno-diorite	20°35'32"	164°30'08"	300	FStp-Act, Ep-Pmp, Pmp-Act, Pmp-Chl		Ap	Pmp-Act
MF3048	diorite	20°35'32"	164°30'08"	300	Pmp-Stp, Ep-Act		Hem, Ap	Pmp-Act
MF3112	basaltic trachyte	20°54'08"	165°12'42"	20	Chl-Stp, Ep-Chl, Chl-Stp-Ms-Ep, Ep-Stp,Chl-Ms	Aug, Ep		Pmp-Act
MF3114	basaltic trachyte	20°53'32"	165°12'00"	10	Ep-Pmp-Chl,Ep-Ms-Pmp-Chl, Ms-Chl, Chl-Ep	Plag		Pmp-Act
MF3155	basaltic andesite	20°47'50"	164°48'10"	100	Chl-Act-Pmp, Pmp-Act, Chl-Act	Aug, Ep, Plag	Calc	Pmp-Act
PS54	metapelite	21°02'08"	165°20'54"	5	Chl-Pmp-Ms			blueschist
PS56	metapelite	21°02'33"	165°21'56"	5	Chl-Ms, Chl-Ms-Pmp, Chl-Ep-Lws-Pmp			blueschist
Poya nappe								
MF3074	basalt	20°18'51"	164°25'01"	180	Chl-Pmp-Ep, Pmp-Chl-Ms-Ep	Aug, Ep	Calc	Pmp-Prh
MF3079	basalt	21°00'15"	165°24'00"	40	Pmp-Chl-Ms-Ep	Aug, Ep	Calc, Hem	Pmp-Prh
MF3084	basalt	21°02'03"	165°23'58"	20	Pmp-Prh	Aug, Plag, Ep	Ap, Calc, Hem	Pmp-Prh
MF3091	basalt	20°45'51"	165°06'45"	20	Chl-Pmp, Chl-Pmp-Act-Ep	Aug, Mg-Hb, Plag		Pmp-Act
MF3092	basalt	20°45'51"	165°06'45"	20	Chl-Pmp	Aug	Ap, Calc	Pmp-Act
MF3095	basalt	20°45'25"	165°07'31"	20	Chl-Pmp-Ep	Aug	Calc	Pmp-Act
MF3106	basalt	20°52'12"	165°14'32"	40	Pmp-Chl-Stp, Pmp-Stp, Ep-Stp, Pmp-Chl, Chl-Stp, Ms	Aug, Ep, Plag	Calc	Pmp-Act
MF3111	basalt	20°53'44"	165°12'53"	20	Chl-Ep-Rbk, Chl-Rbk, Chl-Ep, Chl-Ms	Aug, Ep, Mg-Hb	Calc, Hem	Pm p-Act
MF3113	basaltic trachyte	20°53'50"	165°12'18"	20	Chl-Rbk, Ep-Rbk, Chl-Ep	Ep, Plag	Ap	Pmp-Act
Cretaceous metamorphic zone								
PS76	basaltic andesite	21°17'22"	165°33'53"	20	Pmp-Chl-Ms, Chl-Ep	Aug, Plag, Ep		Pmp-Prh
PS80	basalt	21°22'19"	165°25'29"	100	Chl-Ms,Ep-Ms-Chl, Ep-Ms	Amp, Ep	Calc	Pmp-Prh
PS81	basalt	21°22'38"	165°24'35"	120	Chl-Ms-Ep	Amp, Ep		Pmp-Act
PS46	tuff	21°06'03"	165°17'51"	80	Chl-Ms, Chl-Lws-Pmp	Ep		Pmp-Act
MF3124	basalt	21°29'00"	165°46'32"	50	Ms-Chl-Ep, Chl-Ep, Ms-Chl	Ep, Plag		Prh-Pmp
MF3134	basalt	21°22'27"	165°25'00"	100	Rbk-Chl-Ep, Rbk-Chl, Ep-Chl	Aug		Pmp-Act

Methods

The character of mafic phyllosilicate minerals present in metabasites was determined using a variety of methods including optical microscopy, XRD and EMPA analysis. Whole rock composition of major elements was determined by XRF. Mineral abbreviations used in this study follow KRETZ (1983).

ANALYTICAL METHODS

Chemical analyses of minerals were obtained using wavelength-dispersive spectroscopy on a JEOL JXA-8600 superprobe with NORAN automatization and a PROZA correction program. In order to avoid volatilisation of light elements, low grade metamorphic minerals were analysed using a 10 nA beam current, an accelerating voltage of 15 kV, an acquisition time of 60 seconds and a rastered beam across an area of approx. 25 μm^2.

Minerals were also characterised with a D5000 Bruker-AXS (Siemens) diffractometer, using CuKα radiation, an accelerating voltage of 40 V, a current of 30 mA, automatic divergence slits (primary and secondary V20) with a secondary graphite monochromator.

Analysis of major elements was done with Tracor Spectrace-5000 energy-dispersive X-ray fluorescence equipment.

THERMODYNAMIC MODELLING

Equilibrium assemblages and equilibrium phase diagrams were calculated using the DOMINO-THERIAK software (DE CAPITANI and BROWN, 1987; DE CAPITANI, 1994) to investigate the potential effects of temperature, whole rock composition and oxygen activity on the chemical composition of pumpellyite and associated minerals.

The internally consistent mineral database JUNE92 of BERMAN (1988) was supplemented with thermodynamic data for Fe- and Mg-glaucophane from EL-SHAZLY and LIOU (1991) and Mg-pumpellyite data from EVANS (1990). Data for Fe-pumpellyite were not available, but, SCHIFFMAN and LIOU (1983) determined its cell-volume, and LIOU (1979) bracketed the breakdown reaction 4Fe-Pmp + O_2 = 8Ep + 10W. C_p was estimated according to BERMAN and BROWN (1985). Compressibilities and expansivities were assumed to be equal to those for Mg-pumpellyite. The entropy and the enthalpy of Fe-pumpellyite were derived using these data.

Table 2 Thermodynamic properties of end-members that are updated or not published in the JUN92.
$Cp = k_0 - k_1T^{-0.5} - k_2T^{-2} + k_3T^{-3} + k_6T^2$ JK^{-1}; $V(P/T)/V(1,298.15) = 1 + v_1(T-298.15) + v_2(T-298.15)^2 + v_3(P-1) + v_4(P-1)^2$
Units are in J, K and bar, v_1, v_2, v_3 terms need to be divided by 10^5, v_4 by 10^8.

Mineral	Formula	Comments	H° (J) k_0 v_1	S° (J/K) k_1 v_2	V° (J/bar) k_2 v_3	k_3 v_4	k_6
Fe–Pumpellyite	$Ca_4Al_4Fe_1Fe_1Si_6O_{21}(OH)_7$	(1)	–13612835.00	666.67	29.99		
			1612.3	–11089.12	–24553960.00	3324677000	0.00000
			3.467	0.00000	5.1516	1.288	
Mg–Pumpellyite	$Ca_4Al_4Mg_2Si_6O_{21}(OH)_7$	(2)	–14402300.00	584.00	29.55		
			1576.0	–10603.0	–28304200.00	3838351000	0.00000
			3.467	0.00000	5.1516	1.288	
Mg–glaucophane	$Na_2Mg_3Al_2Si_8O_{22}(OH)_2$	(3)	–11958865.00	535.00	26.05		
			1717.500	–19272.000	7075000.0	0.00000	–0.1210700
			2.71035000	–0.0001500	–0.10959000	0.00000	
Fe–glaucophane	$Na_2Fe_3Al_2Si_8O_{22}(OH)_2$	(3)	–10897567.00	624.00	26.59		
			1762.900	–20207.100	9423700.00	0.00000	0.00000
			3.04625799	0.00000	–0.11658518	0.00000	
Laumontite	$CaAl_2Si_4O_{12}(H_2O)_4$	(1)	–7261180.50	463.33	20.37		
			917.377	–6131.500	–14805540.00	2022583000	0.00000
			2.610028122	–0.000203757	–0.067858953	0.000260199	

(1) this study; (2) Properties derived by EVANS (1990); (3) Properties derived by EL-SHAZLEY and LIOU (1991).

Solution model:

Epidote-Clinozoisite: ideal one site mixing

$a_{Ep} = X_{Fe}{}^{M}$

$a_{Czo} = X_{Al}{}^{M}$

Pumpellyite-Fe Pumpellyite: ideal one site mixing

$a_{Pmp} = X_{Pmp}$

$a_{Fe\text{-}Pmp} = X_{Fe\text{-}Pmp}$

Derived thermodynamic data of Fe-pumpellyite are presented in Table 2, together with all phases not included in the Berman database JUN92.

Results on samples

COMPOSITIONS AND MINERAL ASSEMBLAGES

One of the main problems in the metamorphism of low-grade metamorphic rocks (metabasites or metapelites) is to determine the stable mineral assemblage. Evidence of disequilibrium is common in thin sections. Preservation of incompletely replaced relics of augite and hornblende, intergrain inhomogeneity in the same sample and zoned amphibole are all indicators of disequilibrium. However, local equilibria may be preserved if the metamorphic minerals are in physical contact, provided these grains are unzoned. In the same rock, minerals from veins and host rocks are not necessarily in equilibrium and may be part of a different mineral assemblage. We attempted to identify and study equilibrium assemblages solely on the contact relationships between minerals.

Sample locations are indicated in Fig. 2. The following mineral associations were found in metabasites (Table 1): (1) chlorite-pumpellyite, (2) pumpellyite-chlorite-lawsonite, (3) pumpellyite-chlorite-actinolite, (4) pumpellyite-chlorite-Fe richterite, (5) pumpellyite-chlorite-Fe stilpnomelane, (6) pumpellyite-prehnite. Assemblages (1) and (6) are mainly found in rocks metamorphosed under prehnite-pumpellyite facies conditions. Assemblages (2), (3), (4) and (5) are considered to represent pumpellyite-actinolite facies conditions. In metapelites and the tuff sample, only the assemblages (1) and (2) are observed.

Chlorite

Chlorite is ubiquitous in all metabasites studied. It occurs in veins, as irregular patches in plagioclase, and replaces pyroxene and igneous amphibole (brown hornblende). Its abundance is variable and ranges between 5 and 20 vol% of the rock. The colour of chlorite ranges from colourless to green-yellow; the birefringence colour is violet/blue (most samples), although in some cases brown or violet/blue and brown.

Chemical analyses of chlorite are given in Table 3. The compositions were normalised to 28

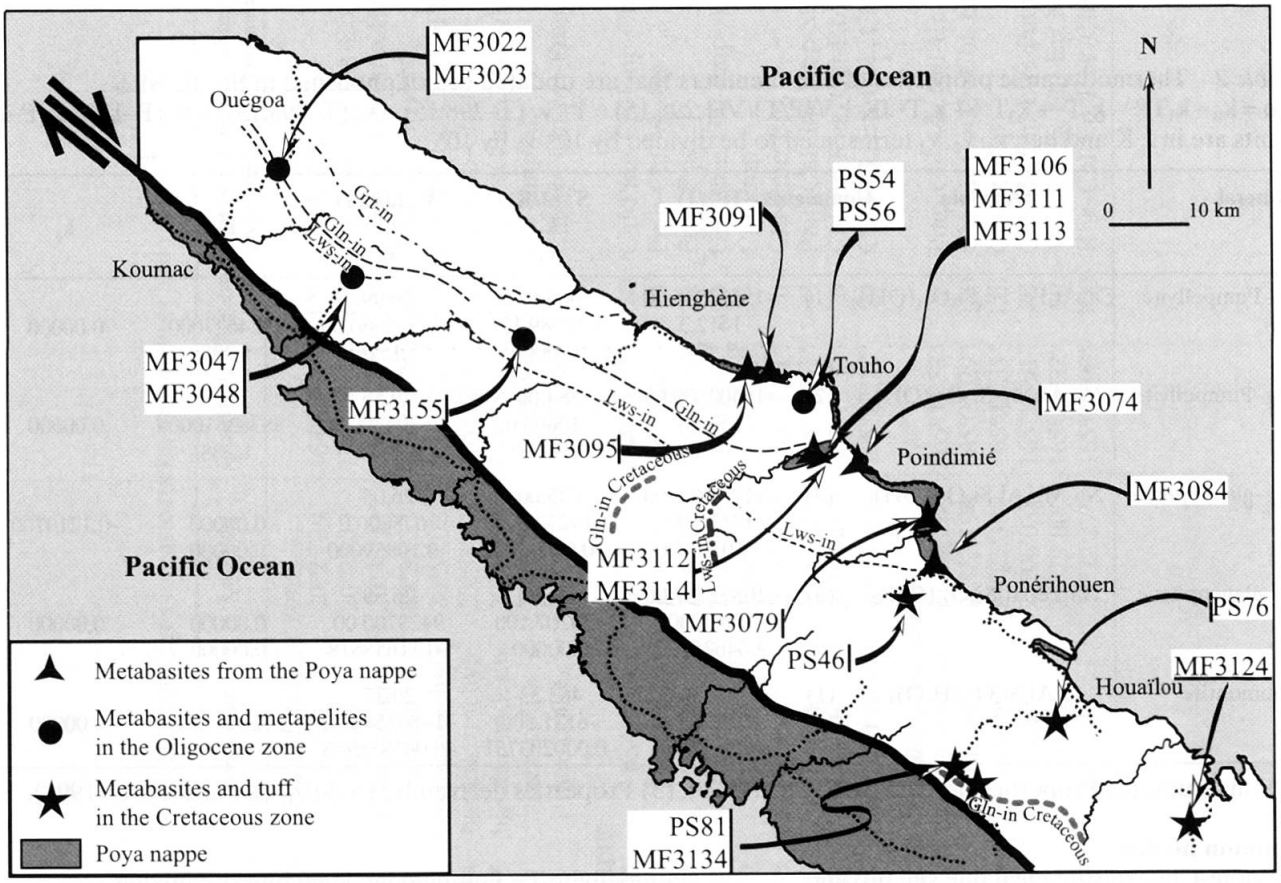

Fig. 2 Location in northern New Caledonia of metabasites, metapelites and one metatuff samples studied. Samples are located in the two metamorphic zones and in the Poya nappe.

oxygens and fulfill the criterion $\Sigma Ca+Na+K < 0.2$ (SCHMIDT et al., 1997) used as a test for microprobe analyses not contaminated by other phases. In a diagram of non-interlayer cations versus Al_{total} the chlorite analyses scatter between 4.0 and 6.2 Al_{total} with no visible trend (Fig. 3). MgO/(MgO+FeO) values for chlorite in metabasites range from 0.35 to 0.90. This ratio has been repeatedly shown to correlate with the same ratio for the whole rock composition (Table 4) (BEVINS and MERRIMAN, 1988; BEIERSDORFER and DAY, 1995). However, the composition of chlorite, for the samples from New Caledonia, does not correlate with the bulk rock composition,

Table 3 Representative microprobe analyses of chlorite in basic rocks, metapelites and one tuff in New Caledonia. Calculations are based on 28 oxygens, and total Fe is assumed to be FeO.

Sample N°	PS76 12 analyses		MF3079 5 analyses		MF3074 16 analyses		MF3092 5 analyses		MF3047 7 analyses		MF3106 21 analyses		PS81 7 analyses		MF3111 58 analyses	
	Mean Values	Std Dev.	Mean Values	Std Dev.	Mean Values	Std Dev.	Mean Values	Std Dev.	Mean Values	Std Dev.	Mean Values	Std Dev.	Mean Values	Std Dev.	Mean Values	Std Dev.
SiO_2	25.21	0.72	27.31	0.44	29.08	0.54	28.38	0.54	26.20	0.66	25.05	0.21	26.16	0.55	25.27	0.75
TiO_2	0.13	0.09	0.08	0.04	0.09	0.14	0.07	0.15	0.02	0.04	0.00	0.01	0.09	0.13	0.23	0.48
Al_2O_3	20.49	0.39	16.52	1.06	18.18	0.23	16.32	0.64	18.19	0.59	17.21	0.73	18.19	0.57	17.58	0.40
FeO	26.01	2.11	26.76	2.58	23.01	0.35	27.22	0.43	28.28	1.34	36.26	1.72	28.29	1.24	31.55	0.45
MnO	0.10	0.16	0.42	0.06	0.38	0.07	0.27	0.08	0.49	0.08	0.52	0.09	0.49	0.07	0.63	0.10
MgO	14.28	1.48	14.91	1.46	19.81	0.33	15.43	0.52	13.78	0.56	8.36	0.24	13.82	0.51	11.34	0.40
CaO	0.09	0.04	0.30	0.17	0.23	0.18	0.21	0.16	0.16	0.12	0.08	0.05	0.18	0.11	0.19	0.23
Na_2O	0.03	0.03	0.04	0.01	0.05	0.10	0.02	0.02	0.03	0.02	0.02	0.02	0.05	0.04	0.07	0.11
K_2O	0.04	0.03	0.13	0.10	0.01	0.02	0.01	0.01	0.02	0.01	0.00	0.01	0.02	0.02	0.02	0.01
Total	86.38		86.47		90.84		87.93		87.17		87.50		87.29		86.88	
Si	5.42		5.91		5.82		6.02		5.67		5.66		5.65		5.61	
Ti	0.02		0.01		0.02		0.01		0.00		0.00		0.01		0.04	
Al	5.20		4.21		4.29		4.08		4.64		4.59		4.63		4.60	
Fe	4.69		4.85		3.85		4.83		5.12		6.85		5.11		5.86	
Mn	0.02		0.08		0.07		0.05		0.09		0.10		0.09		0.12	
Mg	4.58		4.81		5.91		4.88		4.44		2.82		4.45		3.75	
Ca	0.02		0.07		0.05		0.05		0.04		0.02		0.04		0.05	
Na	0.01		0.01		0.02		0.01		0.01		0.01		0.02		0.03	
K	0.01		0.04		0.00		0.00		0.01		0.00		0.01		0.01	
$Mg/(Mg+Fe^{2+})$	0.49		0.50		0.61		0.50		0.46		0.29		0.47		0.39	

Table 3 (continued)

Sample N°	MF3113 15 analyses		MF3091 42 analyses		MF3155 11 analyses		MF3023 15 analyses		MF3114 17 analyses		PS46 11 analyses		PS54 7 analyses		PS56 16 analyses	
	Mean Values	Std Dev.	Mean Values	Std Dev.	Mean Values	Std Dev.	Mean Values	Std Dev.	Mean Values	Std Dev.	Mean Values	Std Dev.	Mean Values	Std Dev.	Mean Values	Std Dev.
SiO_2	24.89	0.43	27.34	0.82	27.83	0.67	30.63	0.63	22.84	0.43	26.06	0.44	29.06	0.70	24.93	0.48
TiO_2	0.05	0.08	0.05	0.06	0.02	0.03	0.02	0.03	0.08	0.08	0.06	0.05	0.07	0.05	0.12	0.12
Al_2O_3	16.39	0.53	16.39	0.53	18.00	0.52	16.52	0.38	19.10	0.59	19.43	0.14	16.98	0.33	19.19	0.51
FeO	33.74	0.86	25.47	0.81	26.04	0.75	12.65	0.90	39.04	0.94	30.54	0.24	19.99	0.46	32.01	0.50
MnO	0.86	0.10	0.26	0.06	0.30	0.06	0.16	0.02	0.58	0.10	0.44	0.07	0.59	0.11	0.51	0.08
MgO	10.44	0.82	16.59	0.55	15.49	0.48	25.91	0.70	4.51	0.26	10.85	0.34	19.30	0.46	9.50	0.16
CaO	0.08	0.07	0.12	0.09	0.24	0.12	0.13	0.04	0.07	0.09	0.02	0.03	0.02	0.02	0.06	0.04
Na_2O	0.02	0.02	0.01	0.02	0.04	0.07	0.03	0.02	0.02	0.02	0.03	0.03	0.02	0.01	0.05	0.03
K_2O	0.04	0.03	0.02	0.01	0.03	0.02	0.05	0.05	0.03	0.02	0.03	0.03	0.03	0.02	0.11	0.03
Total	86.50		86.25		87.99		85.27		86.27		87.46		86.04		86.48	
Si	5.64		5.89		5.86		6.13		5.35		5.42		6.06		5.56	
Ti	0.01		0.01		0.00		0.00		0.01		0.01		0.01		0.02	
Al	4.38		4.14		4.47		3.89		5.27		5.35		4.17		5.05	
Fe	6.40		4.59		4.59		2.11		7.65		6.52		3.48		5.97	
Mn	0.17		0.05		0.05		0.03		0.11		0.08		0.10		0.10	
Mg	3.53		5.33		4.86		7.72		1.57		2.51		6.00		3.16	
Ca	0.02		0.03		0.05		0.03		0.02		0.00		0.00		0.01	
Na	0.01		0.01		0.01		0.01		0.01		0.01		0.01		0.02	
K	0.01		0.01		0.01		0.01		0.01		0.02		0.01		0.03	
$Mg/(Mg+Fe^{2+})$	0.36		0.54		0.51		0.79		0.17		0.28		0.63		0.35	

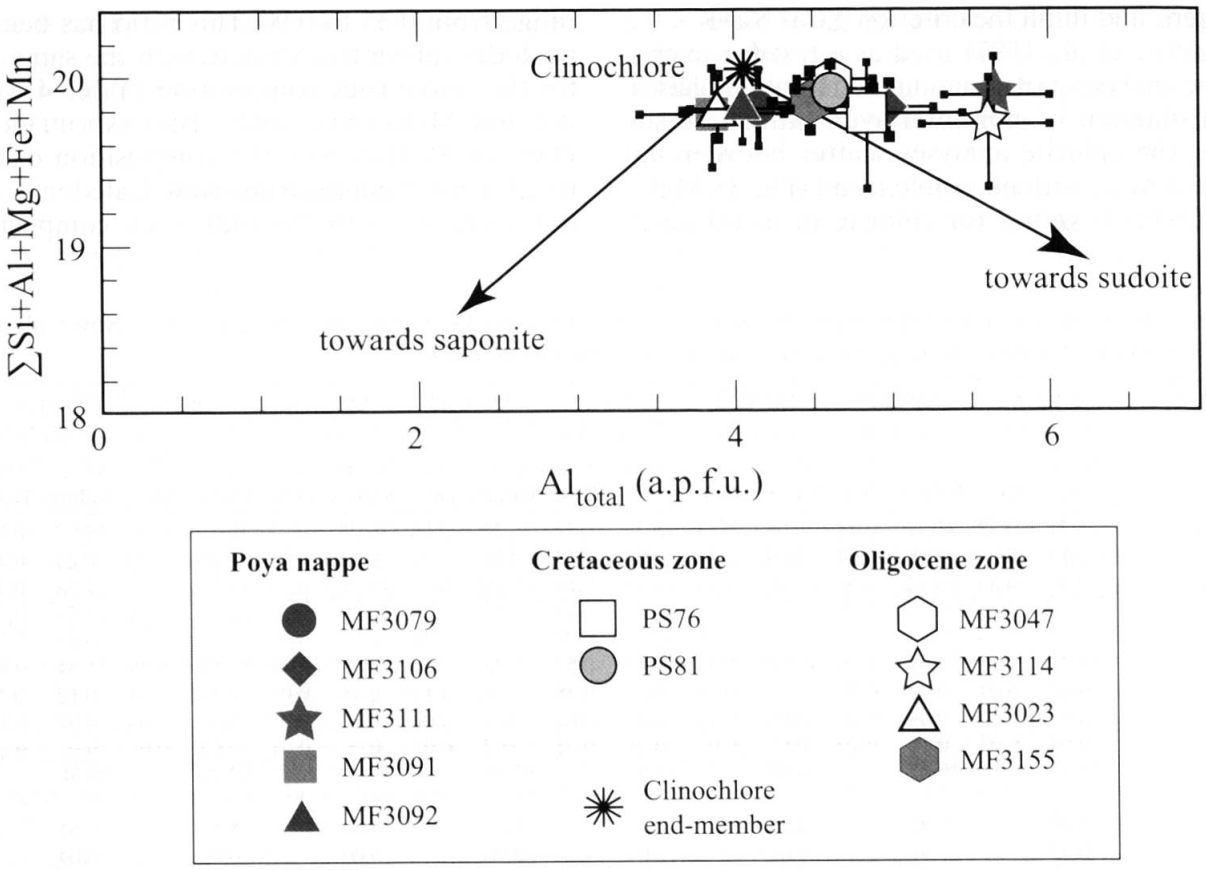

Fig. 3 Average sum of tetrahedral plus octahedral cations, calculated for chlorite analyses from metabasites, plotted against Al_{total}. Analyses cluster close to clinochlore. Error bars (2σ) are represented for each population.

Table 4 Major elements analyses of basic rocks, metapelites and one tuff in New Caledonia.

Sample	MF3022	MF3047	MF3048	MF3112	MF3114	MF3155	MF3074	MF3079	MF3084
SiO_2	44.60	58.31	54.40	56.30	64.56	55.30	49.80	48.26	48.66
TiO_2	0.40	0.87	0.69	1.18	0.75	0.28	0.96	1.39	1.32
Al_2O_3	15.06	17.93	16.60	14.80	15.41	13.30	12.50	13.88	13.75
Fe_2O_3	7.78	5.10	5.29	10.59	5.68	9.54	10.71	11.62	11.02
MnO	0.11	0.00	0.04	0.17	0.13	0.14	0.16	0.18	0.16
MgO	16.14	1.20	1.28	3.38	1.54	5.47	7.54	4.71	7.20
CaO	8.61	6.08	15.71	3.94	2.89	9.91	9.22	12.70	11.32
Na_2O	1.00	7.58	0.93	5.71	4.55	1.96	2.92	3.65	3.22
K_2O	0.24	0.00	0.00	0.58	1.83	0.00	0.03	0.39	0.04
P_2O5	0.00	0.20	0.13	0.28	0.25	0.04	0.09	0.00	0.00
LOI	6.07	2.69	4.41	2.98	2.42	3.95	5.96	3.20	3.31
Total	100.01	99.96	99.48	99.91	100.01	99.89	99.89	99.98	100.00

Sample	MF3091	MF3106	MF3111	MF3113	PS76	PS81	PS54	PS56	PS46
SiO_2	46.39	49.93	51.20	58.50	53.60	47.86	75.70	63.13	59.59
TiO_2	1.20	2.15	1.87	1.36	0.67	2.41	0.50	0.84	0.92
Al_2O_3	14.66	13.61	13.60	13.00	15.37	13.61	9.10	16.05	16.45
Fe_2O_3	11.51	15.04	14.05	11.76	9.61	13.13	4.12	5.83	6.96
MnO	0.16	0.20	0.24	0.25	0.15	0.22	0.09	0.11	0.09
MgO	8.14	4.40	4.59	2.44	6.04	5.79	3.32	1.88	1.99
CaO	11.75	7.01	5.88	4.55	7.63	11.00	1.14	2.97	3.79
Na_2O	2.05	4.93	5.05	5.10	2.89	3.08	0.34	3.15	2.88
K_2O	0.00	0.14	0.31	0.04	1.24	0.14	2.81	2.75	2.35
P_2O_5	0.00	0.23	0.30	0.42	0.00	0.24	0.10	0.23	0.19
LOI	4.14	2.37	2.69	2.46	2.80	2.50	2.67	3.07	4.59
Total	100.00	100.01	99.77	99.88	100.00	99.98	99.89	100.01	99.79

nor with metamorphic grade (R^2 = 0.501, Fig. 4a).

Pumpellyite

Pumpellyite has been found in samples of metabasite and tuff and in one metapelite. It occurs in veins, as aggregates of radially arranged needles in plagioclase and in the matrix. Pumpellyite is usually found in the matrix as well as in the veins of the same specimen, except in metapelites and the tuff. In metabasites and in metapelites, pumpellyite commonly displays brownish or blue-green pleochroism. In the tuff, the crystals show a pleochroism from colourless to olive.

Analyses of pumpellyite (Table 5) were recalculated on the basis of 16 cations per 24.5 oxy-

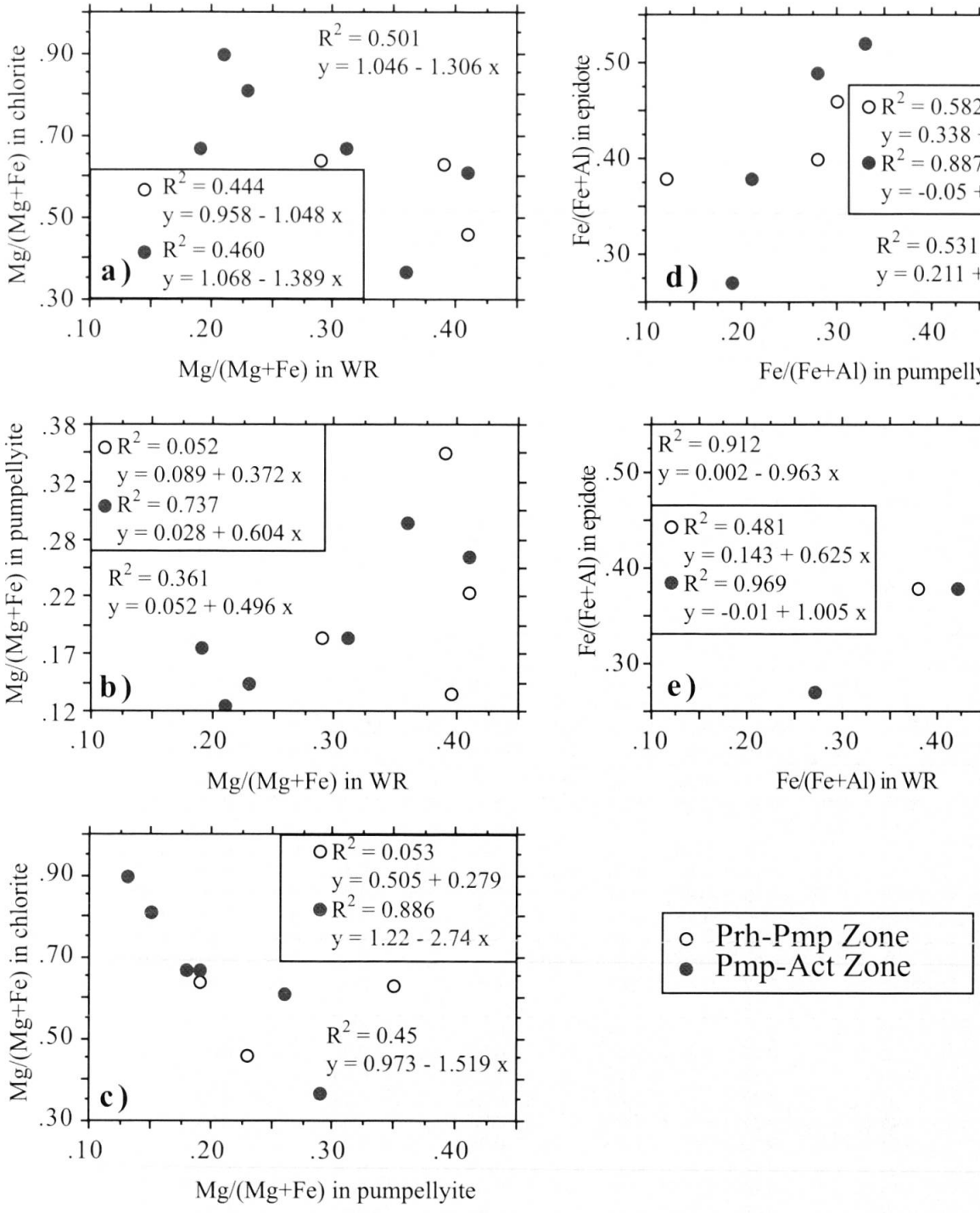

Fig. 4 (a) Correlation between whole-rock composition and chlorite composition in metabasites. (b) Correlation of $MgO/(MgO+Fe_2O_3)$ between whole rock and pumpellyite. (c) Correlation between the MgO/(MgO+FeO) ratio in chlorite and in pumpellyite. (d) Correlation between the MgO/(MgO+FeO) ratio in epidote and in pumpellyite. (e) Correlation of $MgO/(MgO+Fe_2O_3)$ between whole rock and epidote.

gens according to the chemical formula of $W_4X_2Y_4Z_6O_{20+x'}(OH)_{8-x'}$,where x' = 1; W = Ca, Mn; X = Mg, Fe^{2+}, Mn, Al, Fe^{3+}; Y = Al, Fe^{3+}; Z = Si (COOMBS et al., 1976; CORTESOGNO et al., 1984; SPRINGER et al., 1992). The amount of Fe^{3+} in pumpellyite was calculated assuming a chemical formula of $W_4X_2Y_4Z_6O_{21}(OH)_7$; for details see SPRINGER et al. (1992).

Table 5 Representative chemical analyses of pumpellyite. Calculations are based on 16 cations and 24.5 oxygens, and Fe^{3+} and Fe^{2+} were calculated assuming a chemical formula of $W_4X_2Y_4Z_6O_{21}(OH)_7$, and total iron as Fe_2O_3.

Sample N°	PS76		MF3079		MF3074		MF3047		MF3106		PS81		MF3084	
Mineral assemblages	Pmp-Chl 21 analyses		Pmp-Chl 88 analyses		Pmp-Chl 11 analyses		Pmp-Stp 77 analyses		Pmp-Stp 6 analyses		Pmp-Chl 8 analyses		Pmp-Chl 14 analyses	
	Mean Values	Std. Dev.	Mean Values	Std. Dev.	Mean Values	Std. Dev.	Mean Values	Std. Dev.	Mean Values	Std. Dev.	Mean Values	Std Dev.	Mean Values	Std. Dev.
SiO_2	37.15	0.60	37.08	0.48	36.91	0.37	37.76	0.47	35.89	0.49	35.96	0.57	36.62	0.77
TiO_2	0.05	0.06	0.27	0.84	0.08	0.13	0.20	0.25	0.12	0.10	0.10	0.10	0.00	0.00
Al_2O_3	26.71	0.45	22.13	0.68	23.65	0.70	25.30	0.51	22.45	0.61	23.20	1.16	20.70	0.86
FeO	3.42	0.49	9.39	1.00	8.23	1.14	6.85	0.46	9.61	0.47	7.97	1.45	10.82	1.18
MnO	0.00	0.00	0.27	0.07	0.27	0.04	0.06	0.06	0.39	0.04	0.22	0.07	0.12	0.07
MgO	2.03	0.27	2.52	0.37	2.55	0.19	1.65	0.28	1.78	0.17	2.03	0.18	1.77	0.28
CaO	22.18	0.49	20.87	0.77	22.24	0.75	22.03	0.39	21.74	0.38	21.73	0.61	21.50	0.52
Na_2O	0.28	0.21	0.09	0.03	0.10	0.02	0.09	0.02	0.13	0.02	0.09	0.07	0.07	0.02
K_2O	0.06	0.02	0.07	0.20	0.02	0.01	0.01	0.02	0.03	0.03	0.03	0.07	0.02	0.01
Total	91.88		92.69		94.05		93.95		92.13		91.33		91.62	
Si	6.01		6.07		5.92		6.06		5.92		5.95		6.10	
Ti	0.01		0.03		0.01		0.02		0.01		0.01		0.00	
Al	5.09		4.27		4.47		4.78		4.36		4.52		4.07	
Fe^{3+}	0.42		0.71		0.39		0.80		0.51		0.51		0.75	
Fe^{2+}	0.04		0.58		0.71		0.12		0.82		0.59		0.75	
Mn	0.00		0.04		0.04		0.01		0.05		0.03		0.02	
Mg	0.49		0.61		0.61		0.40		0.44		0.50		0.44	
Ca	3.84		3.66		3.82		3.78		3.84		3.85		3.84	
Na	0.09		0.03		0.03		0.03		0.04		0.03		0.02	
K	0.01		0.01		0.00		0.00		0.01		0.01		0.00	
$Mg/(Mg+Fe^{2+})$	0.92		0.51		0.46		0.77		0.35		0.46		0.37	
$Fe^{3+}/(Fe^{3+}+Al)$	0.08		0.14		0.08		0.14		0.10		0.10		0.16	
$Fe^{3+}/(Fe^{3+}+Fe^{2+})$	0.91		0.55		0.35		0.87		0.39		0.46		0.50	

Sample N°	MF3091		MF3155		MF3114		PS46		PS54		PS56	
Mineral assemblages	Pmp-Act 11 analyses		Pmp-Act 11 analyses		Pmp-Chl 18 analyses		Pmp-Chl 7 analyses		Pmp-Chl 7 analyses		Pmp-Chl 3 analyses	
	Mean Values	Std. Dev.	Mean Values	Std. Dev.	Mean Values	Std. Dev.	Mean Values	Std Dev.	Mean Values	Std. Dev.	Mean Values	Std. Dev.
SiO_2	37.08	0.41	37.41	0.51	37.42	0.62	37.89	0.52	37.37	1.15	36.03	0.31
TiO_2	0.16	0.09	0.18	0.18	0.04	0.05	0.08	0.10	0.08	0.09	0.15	0.14
Al_2O_3	20.85	1.14	25.37	0.19	27.66	0.46	26.28	0.29	25.22	0.63	26.66	0.44
FeO	8.15	1.48	5.38	0.04	5.15	0.20	3.94	0.33	2.64	0.27	4.32	0.10
MnO	0.19	0.06	0.18	0.01	0.20	0.14	0.36	0.11	0.51	0.13	0.50	0.35
MgO	2.79	0.87	2.16	0.42	0.91	0.21	1.86	0.36	3.04	0.10	1.56	0.60
CaO	20.85	1.04	21.99	1.78	21.54	0.42	21.52	0.30	21.67	0.89	22.33	0.75
Na_2O	0.09	0.03	0.18	0.04	0.10	0.07	0.09	0.02	0.11	0.06	0.08	0.05
K_2O	0.01	0.01	0.02	0.03	0.03	0.03	0.07	0.05	0.08	0.08	0.04	0.02
Total	90.17		92.87		93.05		92.09		90.72		91.67	
Si	6.07		6.03		6.04		6.15		6.11		5.89	
Ti	0.02		0.02		0.01		0.01		0.01		0.02	
Al	4.39		4.82		5.26		5.02		4.86		5.14	
Fe^{3+}	0.67		0.49		0.69		0.53		0.28		0.51	
Fe^{2+}	0.45		0.24		0.00		0.00		0.08		0.08	
Mn	0.03		0.02		0.03		0.05		0.07		0.07	
Mg	0.68		0.52		0.22		0.45		0.74		0.35	
Ca	3.66		3.80		3.72		3.74		3.80		3.91	
Na	0.03		0.05		0.03		0.03		0.03		0.03	
K	0.00		0.00		0.01		0.01		0.02		0.01	
Mg/(Mg+Fe)	0.60		0.68		1.00		1.00		0.90		0.81	
$Fe^{3+}/(Fe^{3+}+Al)$	0.13		0.09		0.12		0.10		0.05		0.09	
$Fe^{3+}/(Fe^{3+}+Fe^{2+})$	0.60		0.67		1.00		1.00		0.77		0.86	

Pumpellyite compositions are shown in an AFM diagram with $Fe_{tot} = Fe^{3+}+Fe^{2+}$ (Fig. 5). Using the classification of PASSAGLIA and GOTTARDI (1973), the pumpellyites fall in the Fe-pumpellyite and Al-pumpellyite fields. $Mg/(Mg+Fe^{3+})$ and $Fe^{3+}/(Fe^{3+}+Al)$ ratios range between 0.37 and 1.00, 0.05 and 0.16, respectively. The highest Al contents are found in samples from the Cretaceous and Oligocene metamorphic zones, whereas samples from the Poya nappe display the lowest values. Pumpellyite in metapelite PS54 is the most magnesian sample, although it still plots in the Al-pumpellyite field. There is a random correlation ($R^2 = 0.052$) between whole rock composition and pumpellyite composition for the prehnite-pumpellyite zone but a significant correlation ($R^2 = 0.737$) is found for the pumpellyite-actinolite zone (Fig. 4b). Similarly, samples from the pumpellyite-actinolite zone show a decrease of MgO in chlorite with a concomitant increase in pumpellyite ($R^2 = 0.886$) (Fig. 4c). A very significant correlation between pumpellyite–whole rock and pumpellyite–chlorite is only observed in rocks of the Pmp-Act zone. This is probably due to disequilibrium in the rocks of the prehnite-pumpellyite zone.

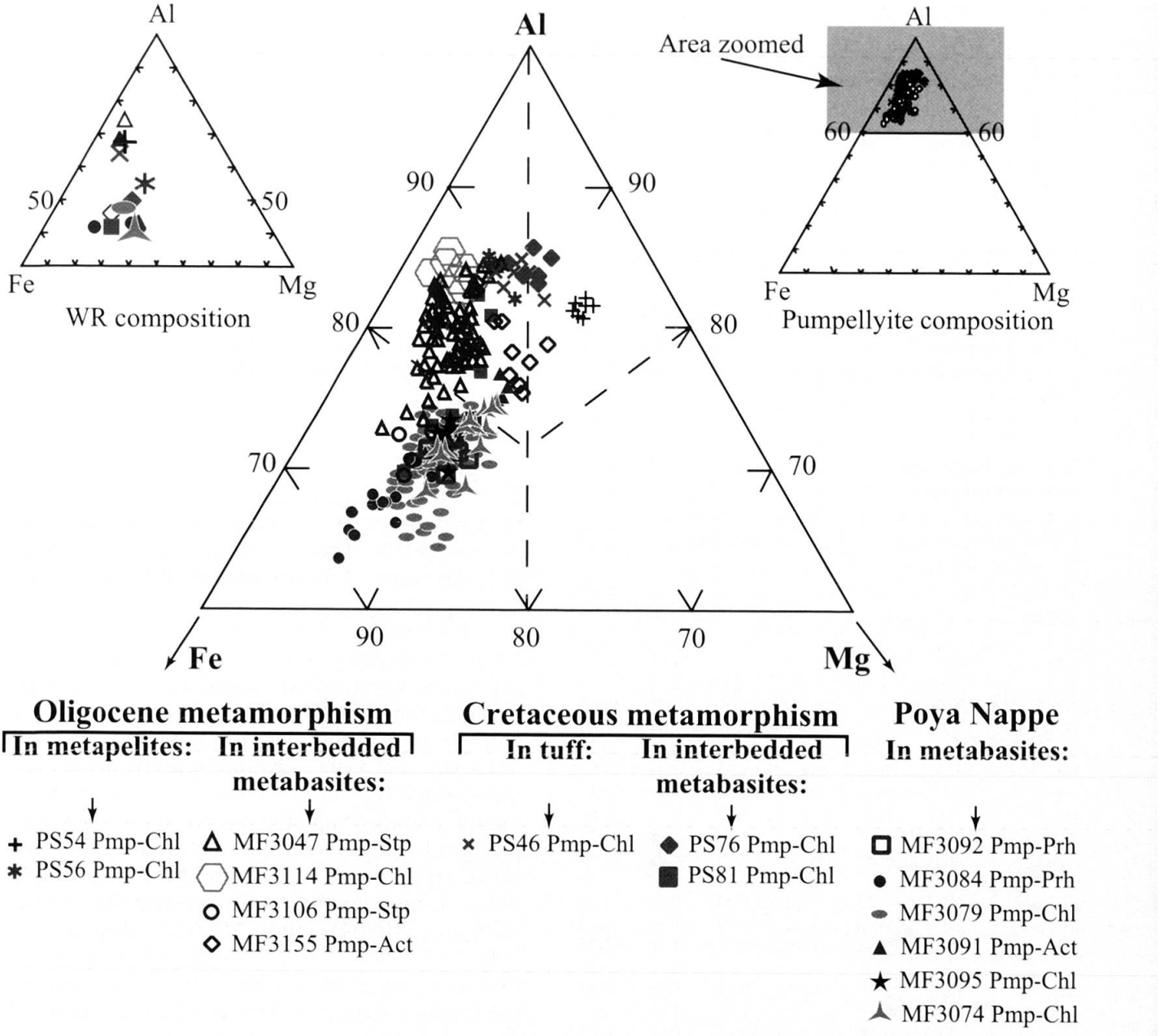

Fig. 5 Fe*–Al–Mg diagram showing pumpellyite compositions from metabasites, metatuffs and the metapelite. The dashed lines in the main diagram indicate different types of pumpellyite (classification of PASSAGLIA and GOTTARDI, 1973). The left hand AFM diagram corresponds to the WR composition of pumpellyite-bearing rocks.

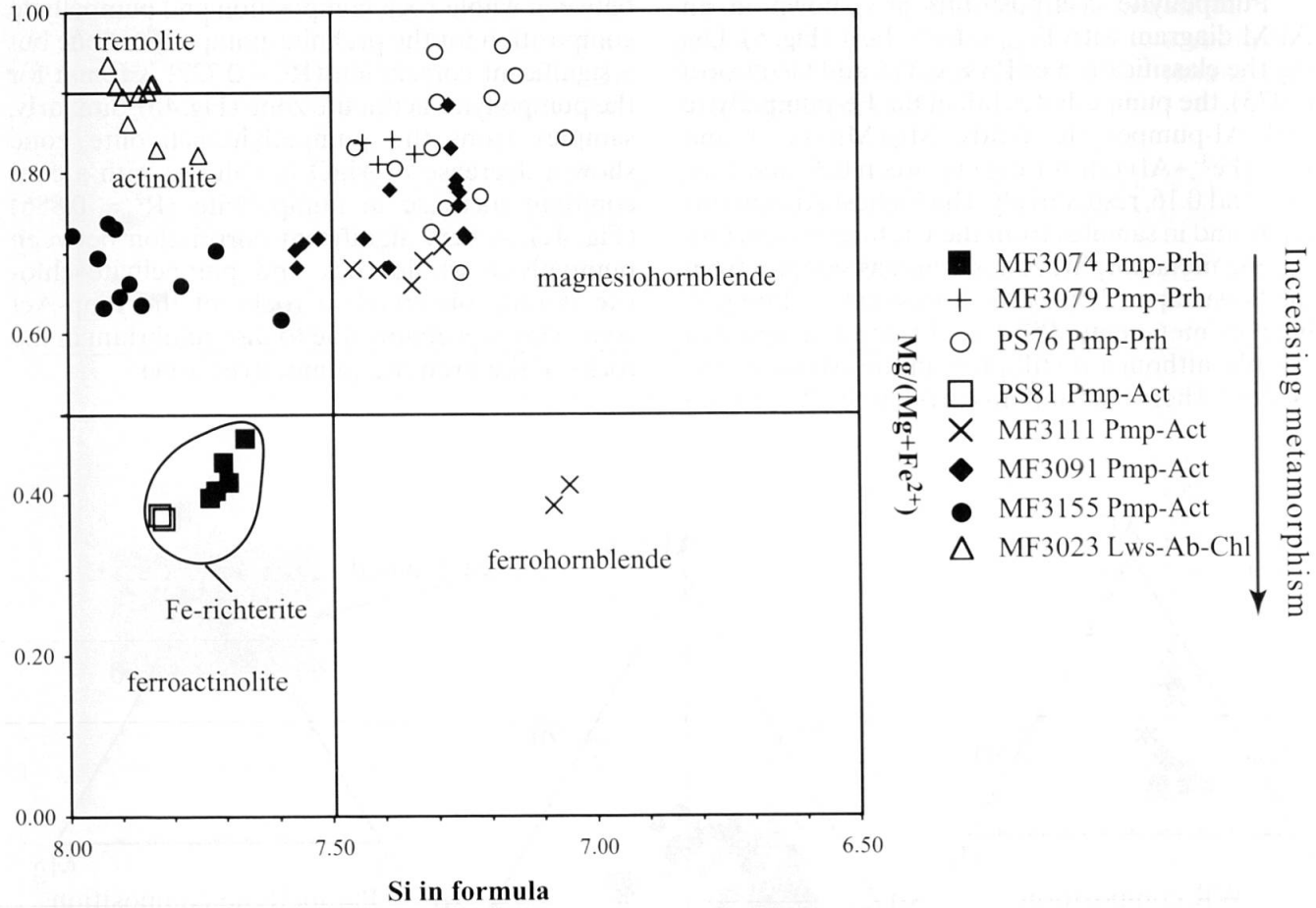

Fig. 6 Mg/(Mg+Fe) versus Si of calcic amphibole from the Prh-Pmp and Prh-Act zones in the study area. Fe-richterite is added in this diagram for comparison, although it is a sodic-calcic amphibole. Classification after LEAKE et al. (1997).

Table 6 Representative chemical analyses of prehnite and Fe-stilpnomelane. Calculations are based on 22 oxygens for prehnite, and the total Fe is assumed to be Fe^{3+}. Calculations for stilpnomelane assume the presence of 8 Si cations, and Fe is calculated as Fe^{2+}.

Sample N°	MF3084 Prehnite		MF3047 Fe-Stp		MF3106 Fe-Stp	
SiO_2	43.82	43.35	45.72	47.39	44.68	43.33
TiO_2	0.00	0.00	0.02	0.00	0.00	0.15
Al_2O_3	20.96	20.11	6.27	6.51	5.91	6.12
FeO	4.05	4.08	29.49	28.98	31.50	31.60
MnO	0.02	0.00	0.28	0.20	0.51	0.72
MgO	0.00	0.00	5.02	5.32	4.03	3.97
CaO	25.72	26.02	0.21	0.30	0.13	0.17
Na_2O	0.04	0.01	0.27	0.12	0.17	0.81
K_2O	0.00	0.02	0.72	0.64	1.28	3.32
Total	94.61	93.59	88.00	89.46	88.21	90.19
Si	6.21	6.22	8.00	8.00	8.00	8.00
Ti	0.00	0.00	0.00	0.00	0.00	0.02
Al	3.50	3.40	1.29	1.30	1.25	1.33
Fe	0.43	0.44	4.31	4.09	4.72	4.88
Mn	0.00	0.00	0.04	0.03	0.08	0.11
Mg	0.00	0.00	1.31	1.34	1.08	1.09
Ca	3.90	4.00	0.04	0.05	0.02	0.03
Na	0.01	0.00	0.10	0.00	0.10	0.30
K	0.00	0.00	0.16	0.14	0.29	0.78
$Mg/(Mg+Fe^{2+})$	0.00	0.00	0.23	0.25	0.19	0.18

Prehnite

Prehnite occurs in a vein (sample MF3084) from the Poya nappe, as anhedral grains with pumpellyite and calcite. Prehnite compositions show Fe/(Fe+Al) ratios of approximately 0.10 (Table 6).

Amphibole

Primary igneous amphibole is anhedral and brown. Newly formed amphibole, replacing pyroxene along rims, is acicular and colourless to pale-green. Amphiboles are classified according to LEAKE et al. (1997). Amphiboles from the prehnite-pumpellyite zone (Table 7) have a Mg-hornblende composition (Fig. 6). At higher metamorphic grade, amphiboles have actinolitic or Fe-richteritic compositions (PS81 and MF3074). Amphiboles found in pumpellyite-actinolite-bearing samples MF3091 and MF3155 display $Mg/(Mg+Fe^{2+})$ ratios of 0.60 and 0.63, respectively (Table 7), which is similar to those of coexisting pumpellyite (0.60 and 0.68, respectively, Table 5).

Table 7 Representative chemical analyses of amphibole. Calculations are based on 23 oxygens. Total iron is assumed to be FeO.

Sample N°	PS76 Mg-hornblende (9)		MF3079 Mg-hornblende (3)		MF3074 Fe-richterite (5)		MF3091 Actinolitic-hornblende (2)		MF3091 Actinolite (17)	
	Mean Values	Std. Dev.	Mean Values	Std. Dev.	Mean Values	Std. Dev.	Mean Values	Std. Dev.	Mean Values	Std. Dev.
SiO_2	49.75	1.35	51.05	0.23	50.33	0.64	50.18	1.14	51.05	0.10
TiO_2	0.33	0.16	0.58	0.23	0.13	0.08	0.19	0.11	0.35	0.11
Al_2O_3	3.98	1.24	2.72	0.40	3.68	0.49	3.72	0.57	3.28	1.15
FeO	17.20	0.75	6.06	0.39	18.45	0.52	17.81	1.15	16.55	0.76
MnO	0.19	0.22	0.20	0.05	0.20	0.04	0.23	0.05	0.16	0.01
MgO	13.79	0.83	16.78	0.47	7.68	0.79	13.39	0.80	13.75	0.23
CaO	10.77	0.99	19.88	0.29	10.74	0.93	10.48	0.43	10.74	0.32
Na_2O	0.36	0.12	0.26	0.01	6.69	0.61	0.78	0.18	0.67	0.17
K_2O	0.09	0.06	0.01	0.01	0.02	0.02	0.10	0.06	0.11	0.03
Total	96.47		97.54		97.92		96.88		96.66	
Si	7.43		7.36		7.60		7.48		7.57	
Ti	0.04		0.06		0.01		0.02		0.04	
Al	0.70		0.46		0.66		0.65		0.57	
Fe	2.15		0.73		2.33		2.22		2.05	
Mn	0.02		0.02		0.03		0.03		0.02	
Mg	3.07		3.61		1.73		2.98		3.04	
Ca	1.72		3.07		1.74		1.67		1.71	
Na	0.10		0.07		1.96		0.22		0.19	
K	0.02		0.00		0.00		0.02		0.02	
$Mg/(Mg+Fe^{2+})$	0.59		0.83		0.43		0.57		0.60	

Sample N°	MF3155 Actinolite (11)		MF3111 Mg-hornblende (7)		MF3111 Fe-hornblende (2)		PS81 Fe-richterite (4)		MF3023 Actinolite (28)	
	Mean Values	Std. Dev.	Mean Values	Std. Dev.	Mean Values	Std. Dev.	Mean Values	Std. Dev.	Mean Values	Std. Dev.
SiO_2	53.92	1.42	49.27	0.97	45.17	0.59	52.20	0.24	55.22	2.88
TiO_2	0.02	0.04	0.57	0.28	0.07	0.09	0.27	0.25	0.08	0.08
Al_2O_3	1.23	0.74	1.80	0.21	4.87	0.20	4.12	0.55	2.14	2.33
FeO	14.99	0.43	11.74	0.57	26.40	0.29	16.32	0.63	7.00	1.43
MnO	0.19	0.08	0.28	0.09	0.68	0.04	0.21	0.10	0.09	0.05
MgO	14.11	0.54	15.22	2.12	6.36	0.12	5.58	0.43	19.35	1.50
CaO	11.37	1.62	18.42	0.51	10.72	0.54	10.65	1.13	11.87	0.46
Na_2O	0.67	0.34	0.42	0.19	0.33	0.01	7.48	0.50	0.97	0.53
K_2O	0.06	0.02	0.01	0.01	0.24	0.05	0.01	0.01	0.05	0.03
Total	96.56		97.73		94.84		96.84		96.77	
Si	7.92		7.29		7.26		7.84		7.80	
Ti	0.00		0.06		0.01		0.01		0.01	
Al	0.21		0.31		0.92		0.70		0.36	
Fe	1.84		1.45		3.55		2.09		0.83	
Mn	0.02		0.04		0.09		0.02		0.01	
Mg	3.09		3.35		1.52		1.24		4.07	
Ca	1.79		2.92		1.85		1.80		1.80	
Na	0.19		0.12		0.10		2.18		0.27	
K	0.01		0.00		0.05		0.00		0.01	
Mg/(Mg+Fe)	0.63		0.70		0.30		0.37		0.83	

Epidote

Epidote is present in the matrix or in veins in most of the rocks (except in the MF3084, PS54 and PS46). It is colourless with yellow interference colours; $Fe^{3+}/(Fe^{3+}+Al)$ ratios (Table 8) range from 0.21 to 0.35, the lowest value being from metapelite PS56 (Oligocene metamorphism). Samples from the highest metamorphic grade dis-

Table 8 Representative chemical analyses of epidote. Calculations are based on 12.5 oxygens. All Fe is assumed to be Fe^{3+}.

Sample N°	PS76		MF3079		MF3074		MF3106		PS81	
	8 analyses		6 analyses		2 analyses		7 analyses		16 analyses	
	Mean Values	Std. Dev.	Mean Values	Std. Dev.	Mean Values	Std. Dev.	Mean Values	Std. Dev.	Mean Values	Std. Dev.
SiO_2	35.29	0.41	36.45	0.31	35.71	0.08	36.69	0.47	37.22	1.34
TiO_2	0.27	0.07	0.05	0.05	0.04	0.06	0.05	0.13	0.25	0.46
Al_2O_3	21.58	1.63	19.53	0.54	22.64	1.46	21.28	0.55	22.51	0.74
Fe_2O_3	16.03	1.60	16.66	0.90	15.27	1.15	16.60	1.16	14.64	0.85
MnO	0.20	0.07	0.03	0.02	0.19	0.01	0.20	0.21	0.18	0.08
MgO	0.06	0.02	0.01	0.01	0.06	0.04	0.01	0.01	0.09	0.16
CaO	20.96	0.44	21.05	0.78	21.50	1.30	21.69	0.89	22.19	0.92
Na_2O	0.02	0.02	0.01	0.01	0.02	0.01	0.02	0.02	0.02	0.02
K_2O	0.00	0.01	0.02	0.01	0.00	0.00	0.00	0.01	0.01	0.01
Total	94.41		93.81		95.43		96.54		97.11	
Si	2.94		3.06		2.94		2.99		3.00	
Ti	0.02		0.00		0.00		0.00		0.01	
Al	2.12		1.93		2.19		2.05		2.14	
Fe^{3+}	1.01		1.05		0.95		1.02		0.89	
Mn	0.01		0.00		0.01		0.01		0.01	
Mg	0.01		0.00		0.01		0.00		0.01	
Ca	1.87		1.89		1.89		1.90		1.91	
Na	0.00		0.00		0.00		0.00		0.00	
K	0.00		0.00		0.00		0.00		0.00	
$Fe^{3+}/(Fe^{3+}+Al)$	0.32		0.35		0.30		0.33		0.29	

Sample N°	MF3155		MF3111		MF3114		MF3113		PS56	
	2 analyses		16 analyses		28 analyses		32 analyses		3 analyses	
	Mean Values	Std. Dev.	Mean Values	Std. Dev.	Mean Values	Std. Dev.	Mean Values	Std. Dev.	Mean Values	Std. Dev.
SiO_2	37.80	0.10	35.88	0.72	36.06	0.96	35.92	0.46	36.67	0.32
TiO_2	0.00	0.00	0.12	0.09	0.10	0.16	0.08	0.12	0.07	0.12
Al_2O_3	23.18	0.28	23.07	1.32	22.15	0.55	19.73	0.65	25.47	1.14
Fe_2O_3	14.29	0.24	14.72	1.45	13.93	1.70	16.34	0.98	10.89	1.41
MnO	0.03	0.00	0.38	0.34	0.27	0.13	0.25	0.26	0.16	0.17
MgO	0.03	0.01	0.11	0.13	0.14	0.24	0.00	0.00	0.04	0.06
CaO	20.56	0.34	21.33	0.91	21.73	1.55	22.27	0.55	23.16	0.36
Na_2O	0.01	0.01	0.03	0.03	0.02	0.02	0.02	0.02	0.03	0.01
K_2O	0.00	0.00	0.01	0.01	0.01	0.01	0.01	0.01	0.06	0.02
Total	95.90		95.65		94.41		94.62		96.55	
Si	3.05		2.94		2.99		3.01		2.94	
Ti	0.00		0.01		0.01		0.01		0.00	
Al	2.21		2.23		2.16		1.95		2.41	
Fe^{3+}	0.87		0.91		0.87		1.03		0.66	
Mn	0.00		0.03		0.02		0.02		0.01	
Mg	0.00		0.01		0.02		0.00		0.00	
Ca	1.78		1.87		1.93		2.00		1.99	
Na	0.00		0.00		0.00		0.00		0.01	
K	0.00		0.00		0.00		0.00		0.01	
$Fe^{3+}/(Fe^{3+}+Al)$	0.28		0.29		0.29		0.35		0.21	

play values less than 0.30 (except in MF3111, where epidote is found in a vein). A plot of FeO/(FeO+Al_2O_3) for pumpellyite versus epidote (Fig. 4d) indicates a well representative correlation (R^2 = 0.531), except in the pumpellyite-actinolite facies (R^2 = 0.887). As observed for pumpellyite, a very significant correlation (R^2 = 0.969) exists between epidote and whole rocks compositions at higher metamorphic grades, where equilibrium may have been reached (Fig. 4e).

Ferro-Stilpnomelane

Ferro-stilpnomelane is observed in some samples from the Oligocene HP metamorphic rocks, both in the matrix, growing as brown to red-brown acicular grains and in some quartz veins. Pumpellyite, chlorite and epidote are associated with Ferro-stilpnomelane. Chemical analyses (Table 6) show that Ferro-stilpnomelane is Fe-rich (Fe/(Fe+Mg) = 0.7–0.8) and occurs in rocks with FeO/(FeO+MgO) ratios higher than 0.7.

MINERAL ASSEMBLAGE AND EQUILIBRIUM

Mineral projections have been used to test for equilibrium between the different mineral assemblages. Because most of the samples contain the association quartz + albite + sphene + epidote, the epidote projection (SPRINGER et al., 1992) was used. Where lawsonite is present (samples MF3023, PS46), a lawsonite projection, similar to that of BRÖCKER and DAY (1995) was used. Several assumptions regarding the Fe^{3+}/Fe^{2+} ratio were used for different minerals: (1) in chlorite, all iron was assumed to be ferrous because the ferric iron contents are usually low in this phase (BEIERSDORFER and DAY, 1995). (2) Iron in epidote is assumed to be entirely ferric. (3) In pumpellyite, iron is present in both states, ferric and ferrous. AIGUIRRE et al. (1995) showed that calculating the FeO/Fe_2O_3 distribution in pumpellyite assuming x'=1 in the ideal pumpellyite formula $W_4X_2Y_4Z_6O_{21}(OH)_7$ provides a good approximation when compared to the FeO/Fe_2O_3 ratio determined by ICP. (4) Ferric iron contents in amphiboles are estimated according to DROOP (1987). The estimated Fe^{3+} contents in chlorite and amphibole reflect the $Mg/(Mg+Fe^{2+})$ ratio in the coexisting phases.

Pumpellyite, epidote and chlorite are virtually ubiquitous in the prehnite-pumpellyite zone, and the assemblage Ep+Pmp+Amp+Chl is observed in gabbroic rocks. In sample PS76, three types of amphibole are distinguished: primary igneous Mg-hornblende (Mg-Hb I) is partly replaced along the rim by Mg-Hb II of very similar composition. A third generation of amphibole is actinolitic in composition and considered to be part of the stable metamorphic assemblage. Pumpellyite occurs in plagioclase associated with newly formed chlorite (Chl I). A second population (Chl II) is found in equilibrium with some pumpellyite and also some newly formed Mg-hornblende (Mg-Hb II). Epidote projections of these samples (Fig. 7) show two different patterns. Pumpellyite is homogenous, whereas $Mg/(Mg+Fe^{2+})$ in chlorite ranges between 0.35 and 0.60, with uniform AF* values. $Mg/(Mg+Fe^{2+})$ of Mg-Hb I and II are between 0.80 and 1.00, with variable AF*. Chl II has the highest $Mg/(Mg+Fe^{2+})$. In sample MF3079 from the Poya nappe, a similar pattern is observed. Pumpellyite shows a uniform composition, whereas chlorite shows a wider compositional range. Two types of amphibole (metamorphic Mg-hornblende and primary Mg-hornblende) are present.

Minerals from rocks of the Pmp-Act facies show less compositional variation (Fig. 8). Chlorite and pumpellyite are homogeneous where they are associated with amphibole. Considering the high variability in mineral compositions and the abundant evidence that equilibrium is attained at small scale only, tie-lines indicate a surprising degree of internal consistency. In most cases, pumpellyite-chlorite tie-lines display a positive slope independent of the PT conditions, even for metapelites and tuffs. In some samples (PS56, MF3091, PS81), pumpellyite displays a wide range of composition, possibly due to disequilibrium.

Different mineral assemblages and different mineral composition have been observed under similar metamorphic PT conditions, and several authors (AIBA, 1982; BANNO, 1964) have shown that rock composition plays an important role on the stable mineral assemblage and the mineral composition. Figure 4e shows a good correlation between the $Fe_{total}/(Fe_{total}+Al)$ ratios of the whole rock and epidote (R^2 = 0.912). The relationship pumpellyite-whole rock (Fig. 4b) displays no correlation, except under Pmp-Act conditions (R^2 = 0.737). Several studies (BANNO, 1964; EVARTS and SCHIFFMAN, 1983; LIOU et al., 1983; CHO et al., 1986; AGUIRRE et al., 1989; DIGEL and NORTON, 1996) have investigated the effect of metamorphic grade on pumpellyite composition. A detailed review by BEIERSDORFER and DAY (1995) identified very different and contradicting trends in pumpellyite composition with metamorphic grade. In metabasites from New Caledonia, the pumpellyite composition displays no simple relationship with metamorphic grade, e.g. the highest and lowest values of the $Fe_{total}/(Fe_{total}+Al)$ ratio are found in samples from the prehnite-pumpellyite facies.

FREY et al. (1991) developed a petrogenetic grid for low-grade metabasites in the NCMASH system. Using this grid as a first approximation, the common occurrence of quartz + pumpellyite + chlorite + actinolite suggests that the temperature did not exceed about 350 °C. Neither laumontite nor other zeolites have been found in our samples suggesting a minimum temperature of 200 °C. Similar metamorphic conditions have been determined by study of the illite crystallinity in the surrounding metapelites (POTEL, 2001).

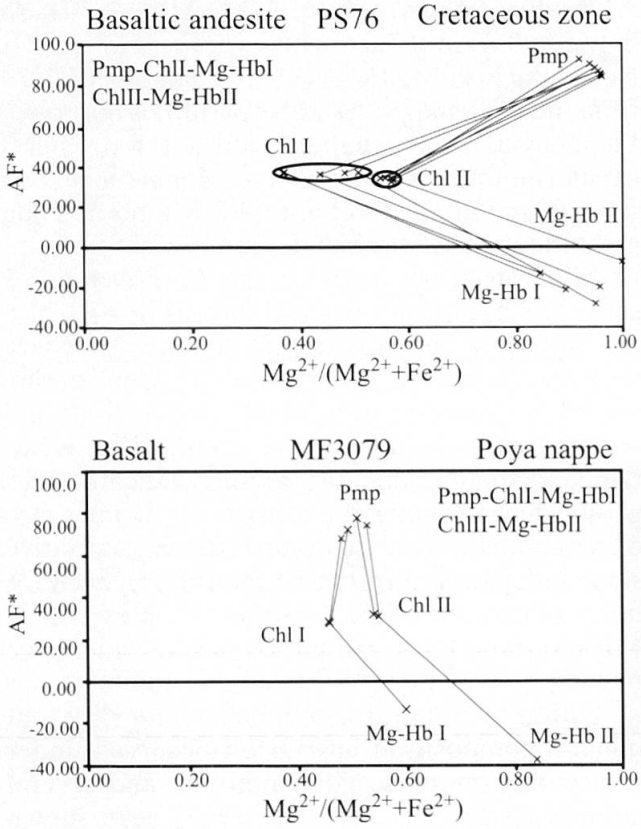

Fig. 7 Mineral assemblages from the Prh-Pmp zone. Projections are from albite-quartz-water-titanite-epidote. $AF^* = 100(Al^{3+}+Fe^{3+}-0.75Ca^{2+}-Na^{+}+0.75Ti^{4+})/(Al^{3+}+Fe^{3+}-0.75Ca^{2+}-Na^{+}+0.75Ti^{4+}Fe^{2+}+Mg^{2+})$.

COMPUTED PHASE DIAGRAMS

Equilibrium phase diagrams were calculated using the DOMINO-THERIAK software to evaluate the effects of whole rock compositions and metamorphic grade on the mineral assemblage and composition of pumpellyite, epidote and chlorite. Three whole rock compositions were chosen, with different values of Al/(Fe+Al) and Mg/(Mg+Fe) (Table 9). These systems are representatives of the whole rock compositions observed in metabasites of New Caledonia. The Al/(Fe+Al) and Mg/(Mg+Fe) ratios are usually assumed to be critical in controlling the composition of minerals. Equilibrium $T-X_{Al}$ and $T-X_{Mg}$ sections were calculated using these rock compositions, with aO_2 buffered by the reaction $H_2 + 3Hem = 2Mag + H_2O$. The epidote-clinozoisite solution is modelled with $a_{Ep} = X_{Fe}{}^{M}$ and $a_{Czo} = X_{Al}{}^{M}$ and the Fe-Mg-pumpellyite solution as ideal ($a_i=X_i$) (Table 2). Calculations for the three different systems were performed at pressures of 3 kbar with the temperature ranging from 100 to 450 °C. These P and T conditions are considered to be common for Prh-Pmp and Pmp-Act facies metamorphism. The temperature range is larger than estimated for New Caledonia in order to accommodate uncertainties in the data and to allow comparisons with other metamorphic belts. The effect of oxygen activity ($T-XaO_2$ section) was investigated for one system. Isopleths of pumpellyite, chlorite and epidote were calculated to show the change in mineral compositions at fixed bulk composition. Each field in Figs. 9–12 represents the stability of a single mineral assemblage.

System 1

Stability fields for pumpellyite, chlorite and epidote are predicted in several assemblages (actinolite, glaucophane and hematite, Figs. 9a–b) for a whole rock composition corresponding to Fe-dominated basaltic rocks, with Mg/(Mg+Fe) = 0.37 and Al/(Fe+Al) = 0.53 (system 1), although the three minerals do not coexist.

In the $T-X_{Mg}$ section (Fig. 9a), pumpellyite has an upper temperature limit of 235 °C, which is independent of whole rock composition. Epidote appears just at the upper temperature limit of pumpellyite. The calculation of the isopleths for pumpellyite ($X_{Al} = 0.1$) and epidote shows negligible variation in composition with increasing temperature or change in whole rock composition. The chlorite isopleths show two trends of compositional variation. At temperatures below 200 °C (glaucophane stable), the isopleths are horizontal and display a decrease in Mg with increasing temperature. Above the glaucophane stability field at temperatures above 200 °C, the Mg-content in chlorite increases with increasing temperature. Chlorite compositions appear to be independent of the Mg/(Mg+Fe) ratio of the whole rock, except in the Act + Pmp + Chl field.

The Al/(Fe+Al) diagram (Fig. 9b) predicts that chlorite, epidote and pumpellyite coexist with laumontite, actinolite and hematite, although the former three minerals do not coexist in a stable situation in any particular field. Chlorite is stable

Table 9 Atom proportion of rock compositions used in the three model systems.

Cations	System1	System2	System3
Si	49.48	45.51	50.33
Al	15.89	16.95	21.66
Fe	11.21	8.50	5.67
Mg	6.50	11.91	1.60
Ca	7.44	12.35	20.06
Na	9.47	3.90	0.00
K	0.00	0.00	0.00
Total	99.99	99.12	99.32
Al/(Fe+Al)	0.59	0.67	0.79
Mg/(Mg+Fe)	0.37	0.58	0.22

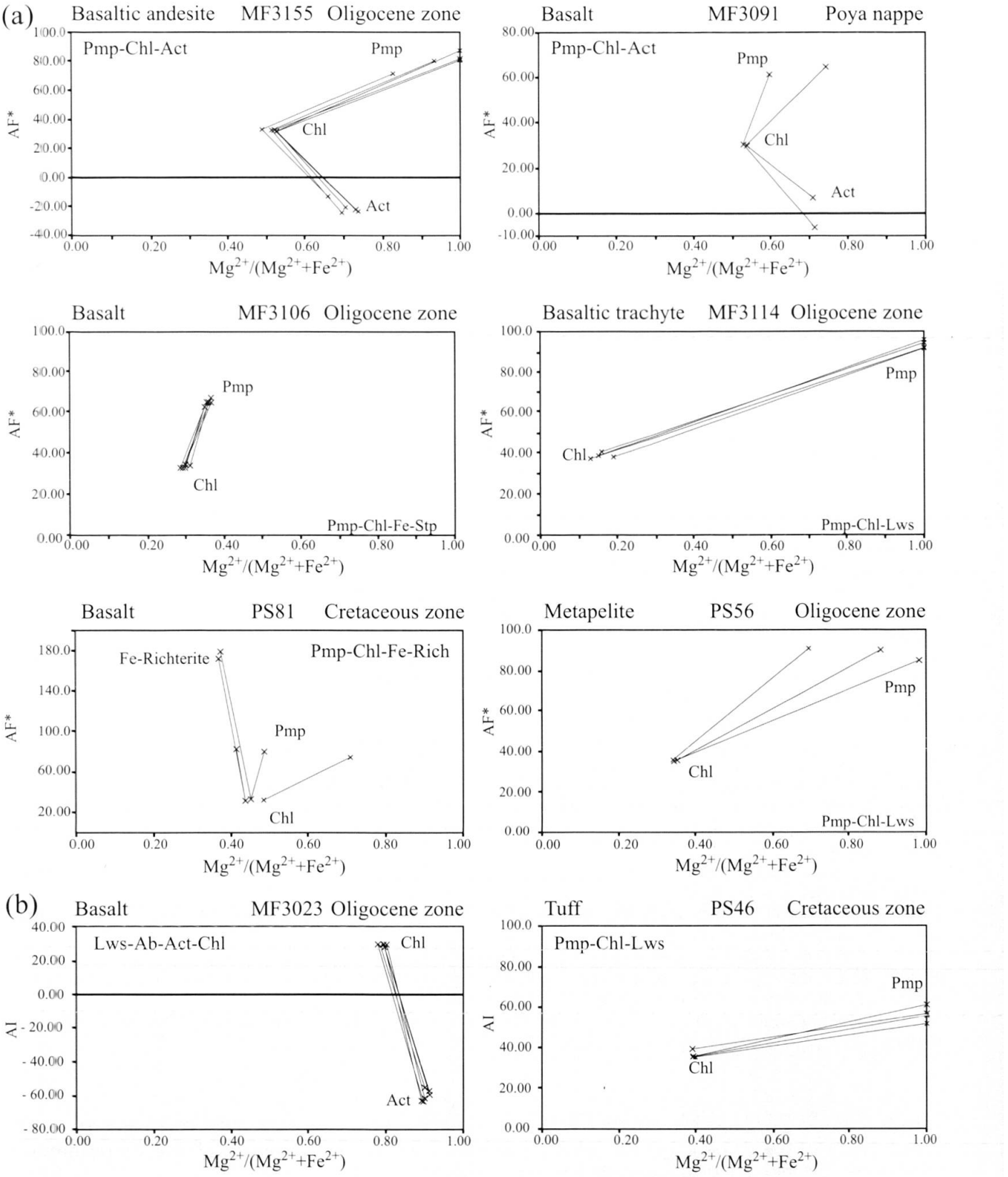

Fig. 8 Mineral assemblages from the Pmp-Act zone. (a) Projections are from albite-quartz-water-titanite-epidote. $AF^* = 100(Al^{3+}+Fe^{3+}-0.75Ca^{2+}-Na^{+}+0.75Ti^{4+})/(Al^{3+}+Fe^{3+}-0.75Ca^{2+}-Na^{+}+0.75Ti^{4+}+Fe^{2+}+Mg^{2+})$. (b) Projections are from albite-quartz-water-lawsonite-hematite. $AI = 100(Al^{3+}-Ca^{2+}-Na^{+})/(Al^{3+}-Ca^{2+}-Na^{+}+Fe^{2+}+Mg^{2+}+Fe^{3+})$.

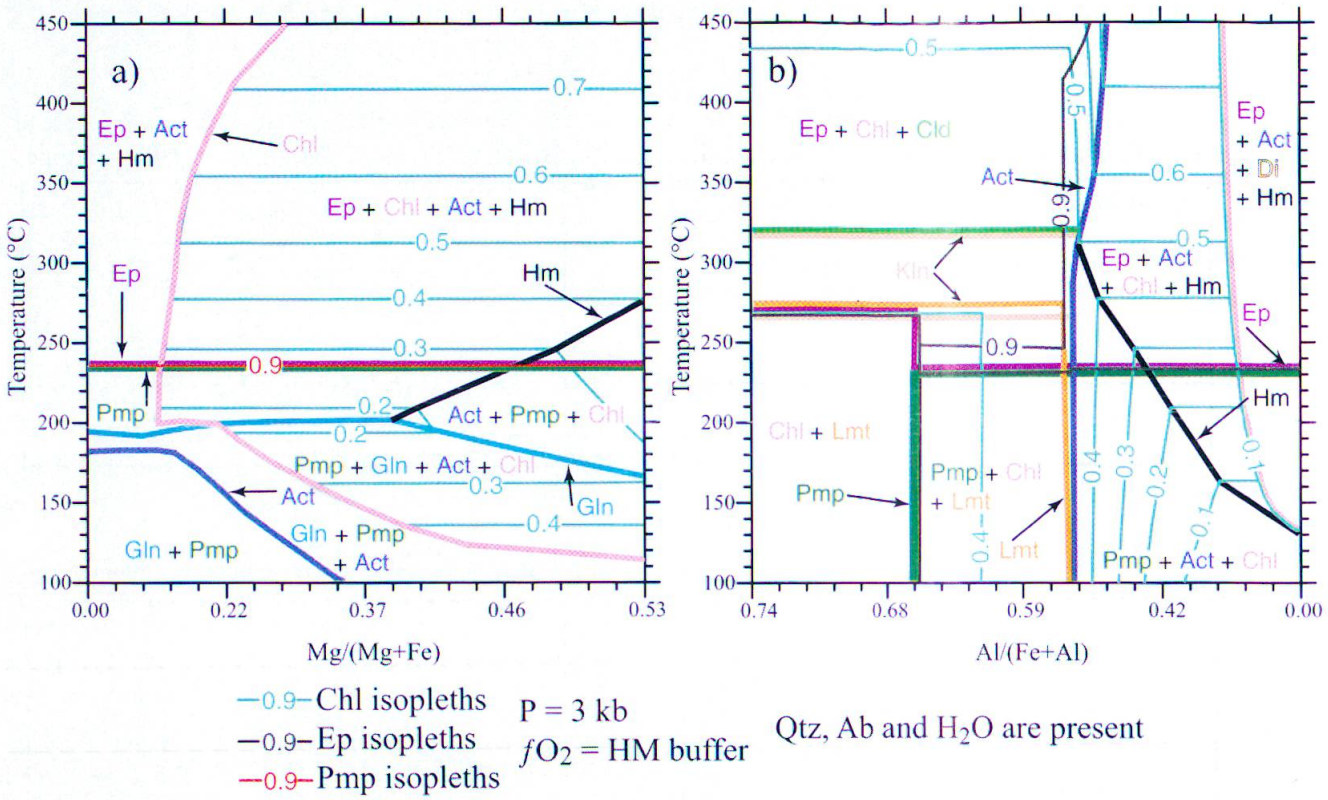

Fig. 9 T–X sections at pressure 3 kbar in a HM-buffered system for rock composition of system 1. The stability fields of the phases are drawn, and isopleths of pumpellyite, epidote and clinochlore have also been plotted when they presented variations in their compositions. Abbreviations are: Ep (epidote), Act (actinolite), Chl (chlorite), Pmp (pumpellyite), Lmt (laumontite) and Gln (glaucophane).
(a) $T–X_{Mg}$ (X_{Mg} = Mg/(Mg+Fe)). Along the x-axis the total molar amount of MgO varies from 13.0 to 0.0. The axis is labeled with calculated values of X(Mg)=Mg/(Mg+Fe) which are non-linearly spaced. The ratio Al/(Fe+Al) remains constant at 0.59.
(b) $T–X_{Al}$ (X_{Al} = Al/(Fe+Al)). Along the x-axis the total molar amount of $AlO_{1.5}$ varies from 31.8 to 0.0. The axis is labeled with calculated values for X(Al)=Al/(Fe+Al). The ration Mg/(Mg+Fe) remains constant at 0.37.

→*Fig. 10* T–X sections at 3 kbar pressure in a HM-buffered system for rock composition of system 2. The stability fields of the phases are drawn, isopleths of epidote, chlorite and pumpellyite are plotted when they presented variations in their compositions. Ep (epidote), Act (actinolite), Chl (chlorite), Di (diopside), Gln (glaucophane) and Pmp (pumpellyite).
(a) $T–X_{Mg}$ (X_{Mg} = Mg/(Mg+Fe)). Along the x-axis the total molar amount of MgO varies from 23.9 to 0.0. The ratio Al/(Fe+Al) remains constant at 0.67.
(b) $T–X_{Al}$ (X_{Al} = Al/(Fe+Al)). Along the x-axis the total molar amount of $AlO_{1.5}$ varies from 0.0 to 33.9. The ratio Mg/(Mg+Fe) remains constant at 0.58.
(c) $T–X_{Mg}$ section at 3 kbar pressure in a HM-buffered system for rock composition of system 2 with X_{Al} = 0.75. The stability fields of the phases are drawn, and isopleths of pumpellyite and epidote are plotted. Ep (epidote), Act (actinolite), Chl (chlorite), Pmp (pumpellyite) and Pg (paragonite).
The total molar amount of $AlO_{1.5}$ is fixed at 33.63. Along the x-axis the total molar amount of MgO varies from 23.9 to 0.0.

→*Fig. 11* $T–X_{Mg}$ section at pressure of 3 kbar in a HM-buffer system for rock composition of system 3. The stability fields of the phases are drawn, and isopleths of pumpellyite, chlorite and epidote are plotted. Ep (epidote), Act (actinolite), Chl (chlorite), Pmp (pumpellyite) and Grt (garnet).
(a) $T–X_{Mg}$ (X_{Mg} = Mg/(Mg+Fe)). Along the x-axis the total molar amount of MgO varies from 3.2 to 0.0. The ratio Al/(Fe+Al) remains constant at 0.79.
(b) $T–X_{Al}$ (X_{Al} = Al/(Fe+Al)). Along the x-axis the total molar amount of $AlO_{1.5}$ varies from 0.0 to 32.5. The ratio Mg/(Mg+Fe) remains constant at 0.22.

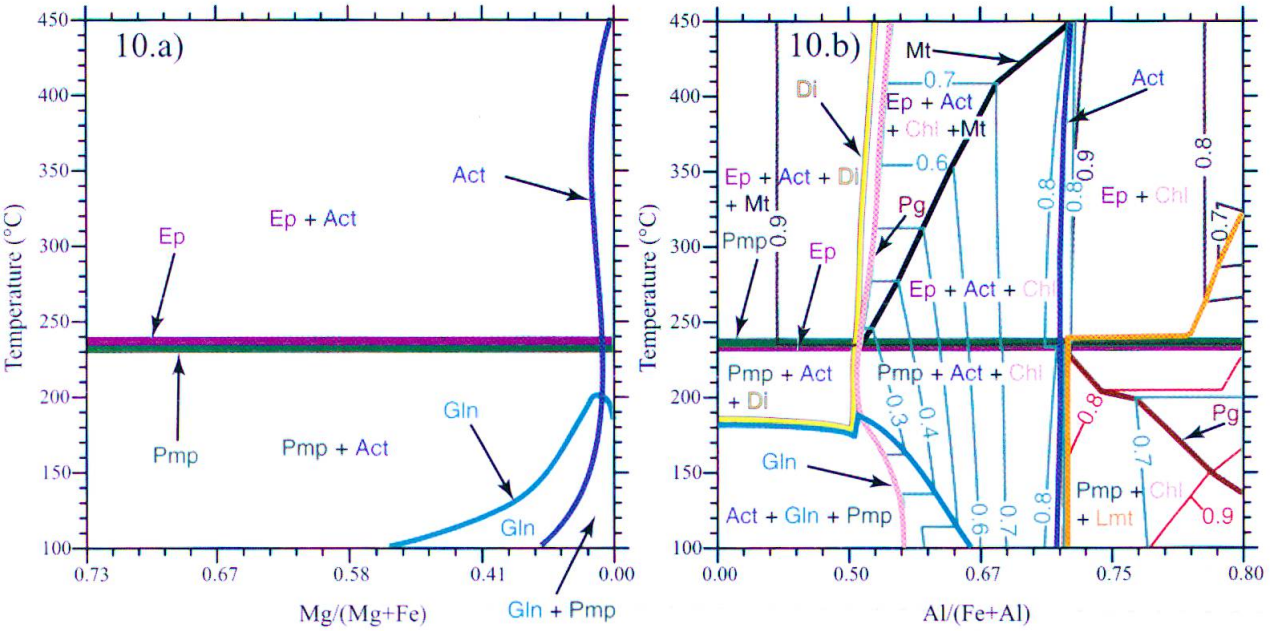

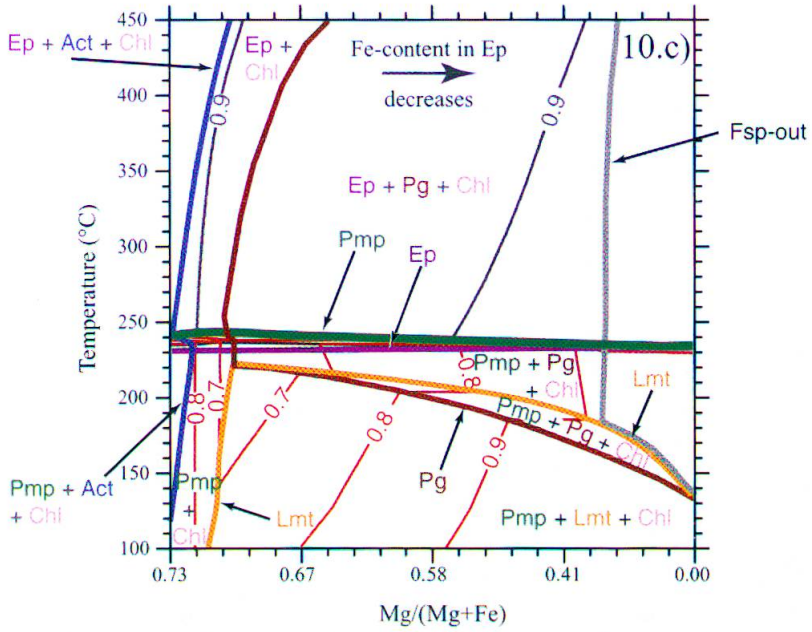

P = 3 kb
fO_2 = HM buffer
—0.9— Chl isopleths
—0.9— Ep isopleths
—0.9— Pmp isopleths

Qtz, Ab and H_2O are present

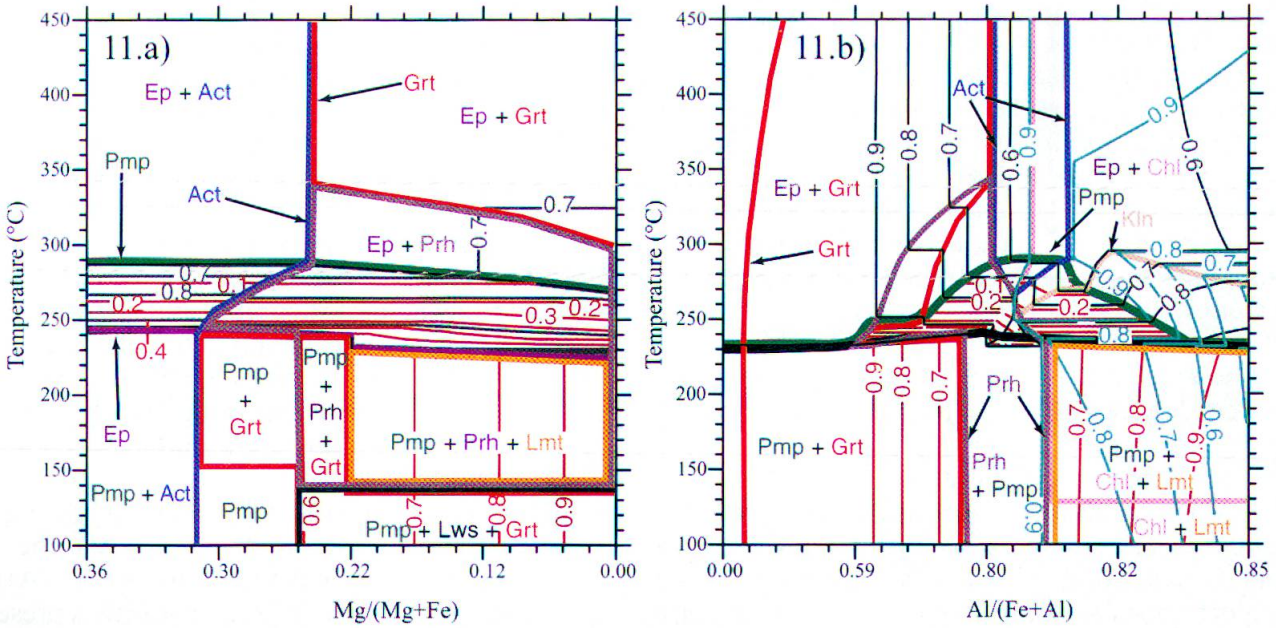

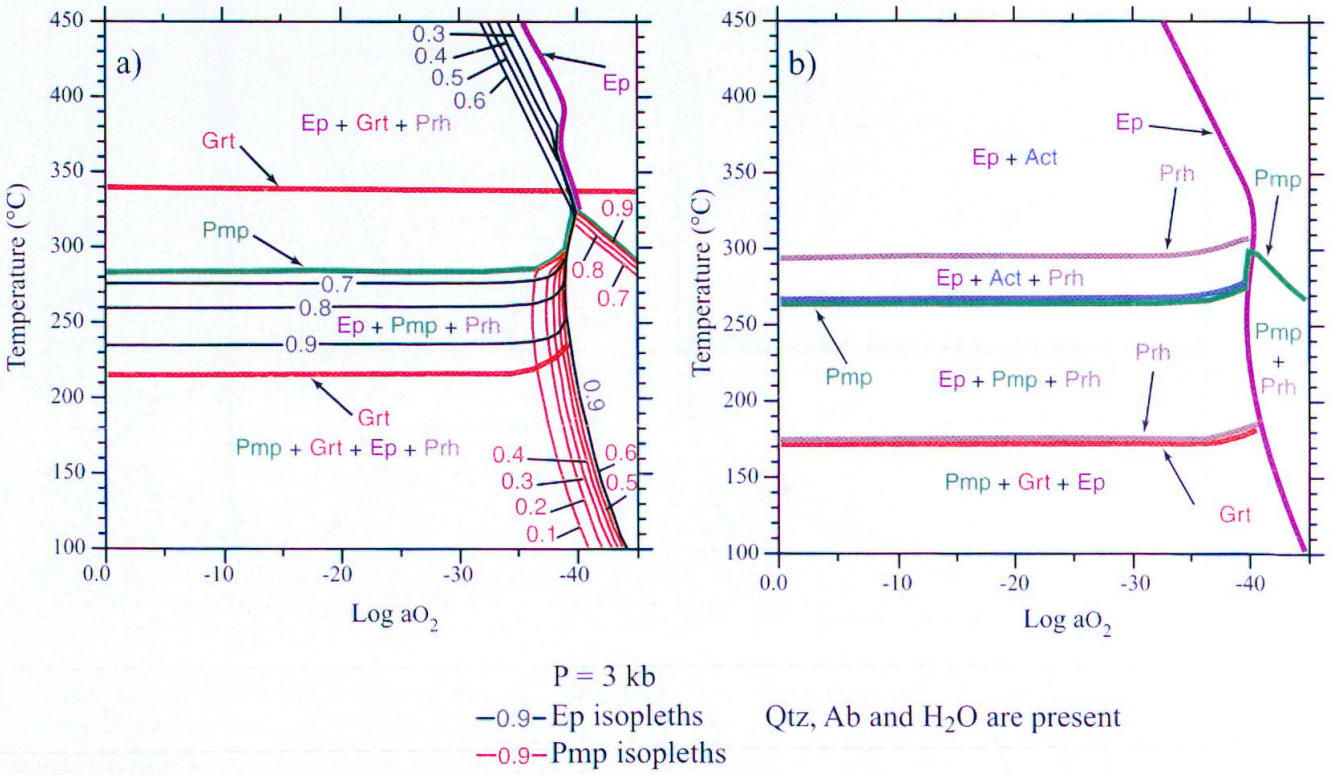

Fig. 12 T–Log aO_2 section at 3 kbar pressure in a HM-buffered system. The stability fields of the phases are drawn, and isopleths of pumpellyite and epidote are also plotted. Ep (epidote), Grt (garnet rich in Ca), Chl (chlorite) and Pmp (pumpellyite). (a) for rock composition of system 3; (b) for rock composition of system 3 with Mg/(Mg+Fe) = 0.26.

over almost the whole diagram and only disappears at Al/(Fe+Al) values below 0.11. Epidote is stable at temperatures above ca. 250 °C. Chlorite isopleths show a complex pattern, which is coupled with the mineral assemblage in equilibrium with chlorite. In the section of the diagram where pumpellyite, actinolite and chlorite are present, the chlorite composition is a function of the Al/(Fe+Al) ratio. In the hematite-bearing field, the Mg content in chlorite increases with temperature and is independent of the Al/(Fe+Al) ratio.

Most of the changes observed in system 1 are controlled by whole rock composition or temperature. Natural assemblages such as Pmp + Act + Chl or Ep + Chl + Act are observed in the modelled system for high values of X_{Mg} or low values of X_{Al}. The coexistence of epidote and pumpellyite is not predicted in this Fe-dominated system.

System 2

System 2 corresponds to a Mg-dominated basaltic composition, characterised by Mg/(Mg+Fe) = 0.58, and a high ratio of Al/(Fe+Al) = 0.67.

At high Mg/(Mg+Fe) values, pumpellyite and actinolite are stable up to 235 °C (Fig. 10a); at higher temperature, pumpellyite disappears and epidote appears. Chlorite is absent in both assemblages. At low Mg/(Mg+Fe) values a different mineral assemblage with glaucophane becomes stable.

Various assemblages are observed in the T–X_{Al} section (Fig. 10b). Chlorite, epidote and pumpellyite are present, but do not coexist. Epidote appears at temperatures above 235 °C. Chlorite is only present where Al/(Fe+Al) < 0.5. Variations in the pumpellyite composition are predicted in the actinolite-absent field ($\approx X_{Al} > 0.73$) where pumpellyite, chlorite and laumontite are present. In this field, the Fe-contents of pumpellyite decrease from 0.9 to 0.8 with increasing temperature. At 235 °C, pumpellyite disappears and epidote appears. In a short temperature interval (<5 °C), the pumpellyite composition changes from $X_{Fe\text{-}Pmp}$ = 0.8 to 0.6.

Figure 10 illustrates which parameters control the chlorite composition. Chlorite composition depends on whole rock composition in the stability field of the assemblages epidote-actinolite-chlorite and pumpellyite-actinolite-chlorite, whereas chlorite composition is controlled solely by temperature in the epidote-actinolite-chlorite-magnetite stability field.

Because pumpellyite only shows bulk compositional variation with high Al/(Fe+Al), the T–X_{Mg} section was also calculated for Al/(Fe+Al) = 0.67 (Fig. 10c). In this diagram, chlorite is present

in all assemblages and shows a Fe-rich composition (X_{Fe} = 0.9). Epidote appears above 240 °C and is independent of X_{Mg}. Pumpellyite and epidote are stable together in a very small field at high Mg/(Mg+Fe) ratios. Isopleths for both minerals are temperature dependent, except where Pmp + Chl + Ep coexist (very small stability field X_{Mg} > 0.5 and approx. 235 °C). Where pumpellyite and epidote coexist, the Fe-contents of pumpellyite decrease while those of epidote increase with increasing temperature. In all the other fields where pumpellyite is stable, its isopleths are clearly controlled by the whole rock composition and affected in their T–X slope by the mineral assemblages. The composition of epidote is quite constant, with variations in Al/(Fe+Al) being <0.1, and practically independent of temperature.

System 2 predicts that pumpellyite and epidote only coexist over a small temperature range and at very particular bulk compositions, not too rich in Fe. As already shown for system 1, actinolite seems to be more characteristic of Fe-rich systems.

System 3

System 3 has low Mg/(Mg+Fe) and high Al/(Fe+Al) ratios of 0.2 and 0.8, respectively, and can still be considered basaltic in composition, with high values of Fe, Ca and Al (Figs. 11a–b).

Rather simple mineral assemblages are observed in the T–X_{Mg} diagram (Fig. 11a), in which associations of Prh + Pmp, Prh + Pmp + Ep and Prh +Ep are predicted. Epidote is stable above 240 °C at high Mg contents and above 230 °C for Mg/(Mg+Fe) < 0.22. Chlorite is absent in this system. Similar to Fig. 10c, pumpellyite and epidote are stable together but over a larger temperature range. For X_{Mg} > 0.25, isopleths of pumpellyite are only controlled by whole rock composition, and the Fe-content of pumpellyite increases with decreasing Mg/(Mg+Fe) ratio. A major change is observed with the appearance of epidote. In the assemblage with epidote the composition of pumpellyite becomes independent of rock composition, but again depends on temperature. Epidote shows a similar behaviour as pumpellyite. It becomes Fe-richer with increasing temperature. Above the pumpellyite stability the epidote isopleths reflect again the whole rock composition.

The interpretation of the T–X_{Al} section is more complex, but similar to Fig. 11a. The lower temperature limit of epidote is still around 240 °C, but the pumpellyite-out reaction is variable and is a function of the composition of the system. Chlorite is only stable at high Al whole rock contents. From Al/(Fe+Al) = 0.1 to 0.75 (prehnite-in), X_{Fe} of pumpellyite decreases from 1 to 0.7. In the assemblage with prehnite, the composition of pumpellyite is constant; in the Pmp + Chl + Lmt field, pumpellyite isopleths are again controlled by bulk composition.

The predicted assemblages show that pumpellyite and epidote can coexist together, in association with either actinolite or prehnite (Fig. 11a). The coexistence of these two minerals expands the stability field of pumpellyite up to 290 °C.

Oxygen activity

On the basis of field observations LIOU (1979) and SCHIFFMAN and LIOU (1983) proposed a dependence of the pumpellyite composition on fO_2. They showed that increasing fO_2 decreases the Fe-content in pumpellyite and increases the Fe^{3+}/Al ratios of coexisting minerals, such as epidote. We investigated this behaviour, calculating the effect of aO_2 on the mineral assemblage and the composition of minerals in system 3. The equilibrium phase diagram (Fig. 12a) obtained shows, in accordance with the observations, a decrease of the Fe-content in pumpellyite and an increase of the Fe-content in epidote with increasing aO_2. An increase in aO_2 increases the stability of pumpellyite for a given Fe content towards higher temperatures. LIOU (1973) described that increasing aO_2 decreases the temperature at which epidote first appears and simultaneously decreases the upper temperature limit of pumpellyite.

The calculations with system 3 yielded no actinolite (Fig. 12a), and hence the Mg/(Mg+Fe) ratio was increased to 0.26. The resulting equilibrium phase diagram (Fig. 12b) shows at low aO_2 the assemblage Prh-Pmp. Increasing the aO_2, two different mineral assemblages become stable: at low temperatures, the assemblage is Pmp-Prh-Ep, at higher temperatures it is replaced by Prh-Act-Ep.

Conclusion

In all three systems investigated, pumpellyite is stable at 3 kbar up to 240 °C, in various mineral assemblages and over a wide range of whole rock compositions. The stability limit of pumpellyite may extend to 290 °C in system 3, at low Mg/(Mg+Fe) and high Al/(Fe+Al) ratios, in a field where pumpellyite and epidote coexist.

The factors that control the pumpellyite composition can vary within any of these systems (e.g. system 3). Pumpellyite composition may be constant over a certain compositional and temperature range because it is buffered by the stable mineral assemblage. Composition of pumpellyite depends on temperature only if other Fe-bearing

minerals are consumed or exchange at the same time. This may explain the contradicting observations made in various field studies (e. g. SPRINGER et al., 1992; BELMAR, 2000). Epidote appears in all 3 systems at temperatures above 240 °C and is critical for the stability of pumpellyite. Epidote and pumpellyite only coexist over a small temperature interval (up to 70 °C) and a narrow range of whole rock composition. The assemblage prehnite-pumpellyite, characteristic of the respective facies, is stable over a small compositional but relatively large temperature range (ca. 130 °C). The pumpellyite-actinolite and pumpellyite-chlorite-actinolite assemblages are generally considered to have formed under higher temperatures than the prehnite-pumpellyite assemblage. Our calculations indicate that the former assemblages are stable in the same temperature range but with lower Al/(Fe+Al) and higher Mg/(Mg+Fe) ratios than the prehnite-pumpellyite assemblage.

The response of pumpellyite composition to bulk rock composition and temperature changes is different in each system. A change in Fe-content at high Al/(Fe+Al) influences the Fe-content of the pumpellyite. This effect is more pronounced when pumpellyite has no mineral to exchange Al, Fe or Mg with. If other Fe-minerals (epidote, chlorite) can buffer the pumpellyite composition, the latter becomes temperature dependent. This behaviour corroborates with the observations made by ISHIZUKA (1991) and CHO (1991) on natural assemblages. It explains why two samples (one with epidote and one without) from New Caledonia with the same metamorphic grade can display two different Mg/(Mg+Fe) ratios in pumpellyite (MF3074 and MF3084).

In all the calculated diagrams, the behaviour of epidote is comparable to pumpellyite. Epidote composition is dependent on temperature, if it can exchange or react with others minerals. CHO et al. (1986) and SCHIFFMAN and LIOU (1983) previously observed this fact in natural assemblages. If epidote cannot react with other minerals, its composition is solely dependent on the bulk composition.

The effect of aO_2 should not be neglected, as shown in Figs. 12a–b. For a given bulk composition, variations in aO_2 can lead to the coexistence of minerals that are not stable together otherwise.

Assemblages used to define typical mineral facies of (very) low-grade metamorphism such as Pmp-Act, Pmp-Prh and Ep-Act are present in the modelled systems. These assemblages are largely controlled by the composition of the whole rock. Mineral assemblages comprising actinolite are found in rocks with high Mg/(Mg+Fe) ratios. Associations of Ep and Prh are only observed at high values of aO_2 in Fig. 12a. BEVINS and MERRIMAN (1988) described Prh-Ep-Pmp assemblages from North Wales in zones that are characterised by a high Fe_2O_3 content. Other mineral assemblages involving Prh, Act and Ep are predicted in Fig. 12b, at higher Mg/(Mg+Fe) ratio and high values of aO_2.

These results represent a first attempt to determine the factors that control the compositions of pumpellyite and epidote. Whereas thermodynamic calculations represent equilibrium states, metabasites at low-grade conditions may only achieve such a state at a small-scale. When applying these calculations, the presence of igneous mineral relics needs to be taken into account, to avoid erroneous interpretations of the composition of different newly grown minerals. For example, ignoring the presence of amphibole relics will lead to an excess of Ca, Al, Fe, Mg in a model composition and this may generate minerals that are not observed in the natural assemblage.

In conclusion, host rock composition, aO_2 and the mineral association collectively control the composition of pumpellyite, chlorite and epidote. Attempts to use their compositions as a facies indicator or to deduce implications for the geotectonic setting must therefore be considered with caution.

Acknowledgements

This research was supported by grant 20-56842.99 of the Swiss National Research Foundation. R. M. Le Bayon is thanked for fruitful discussions about DOMINO-THERIAK and thermodynamic data. W. Tschudin and H. Hürlimann are thanked for the preparation of thin sections and whole-rock analyses, respectively. W. Stern is thanked for the bulk composition analyses and discussions. We thank R. Ferreiro Mählmann for numerous suggestions during the preparation of this paper and R. Spikings for reading and correcting the English of the last version. We are also very thankful to P. Nievergelt for careful handling of the pre-press work of our paper. The manuscript benefited from a thorough review and constructive comments by M. Engi, which is thankfully acknowledged. We are also very thankful to Prof. Martin Frey, the former head of the department in Basel, to whom we dedicate this paper: Many stimulating discussions and field trips in the Swiss Alps helped us to deepen our understanding of low-grade metamorphism.

References

AGUIRRE, L. (1993): Compositional variations of Cretaceous pumpellyites along the western margin of South America and their relation to an extensional geodynamic setting. J. Metamorphic Geol. 11, 437–448.

AGUIRRE, L., LEVI, B. and NYSTROM, J.O. (1989): The link between metamorphism, volcanism and geotec-

tonic setting during the evolution of the Andes. In: DALY, J.S., CLIFF, R.A. and YARDLEY, B.W.D. (eds): Evolution of metamorphic belts. Geol. Soc. London Spec. Publ. 43, 223–232.

AGUIRRE, L., MORATA, D., PUGA, E., BARONNET, A. and BEIERSDORFER, R.E. (1995): Chemistry and crystal characteristics of pumpellyite in a metadolerite from the Archidona region, Subbetic Cordillera, Spain. In: SCHIFFMAN, P. and DAY, H.W.,(eds): Low-Grade Metamorphism of Mafic Rocks: Boulder, Colorado. Geol. Soc. Am. Spec. Paper 296, 171–181.

AITCHISON, J.C., CLARKE, G.L., MEFFRE, S. and CLUZEL, D. (1995): Eocene arc-continent collision in New Caledonia and implications for regional southwest Pacific tectonic evolution. Geology 23, 161–164.

AITCHISON, J.C., IRELAND, T.R., CLARKE, G.L., CLUZEL, D. and MEFFRE, S. (1998): U/Pb SHRIMP age constraints on the tectonic evolution of New Caledonia and regional implications. Tectonophysics 299, 333–343.

AIBA, K. (1982): Sanbagawa metamorphism of the Nakatsu-Nanokawa district, the northern subbelt of the Chichibu belt in western central, Shikoku. Geol. Soc. Japan Journal 72, 253–265.

BANNO, S. (1964): Petrologic studies on Sanbagawa crystalline schists in the Bessi-Ino district, central Sikoku, Japan. Tokyo University Faculty of Science Journal 15, 203–319.

BEIERSDORFER, R.E. and DAY, H.W. (1995): Mineral paragenesis of pumpellyite in low-grade mafic rocks. Geol. Soc. Am. Spec. Paper 296, 5–27.

BELMAR, M. (2000): Low-grade metamorphism in Central Chile at 35°S. PhD thesis, Basel, 190 pp.

BERMAN, R.G. and BROWN, T.H. (1985): Heat capacity in the system Na_2O-K_2O-CaO-MgO-FeO-Fe_2O_3-Al_2O_3-SiO_2-TiO_2-H_2O-CO_2: representation, estimation, and high temperature extrapolation. Contrib. Mineral. Petrol. 89, 168–183.

BERMAN, R.G. (1988): Internally-consistent thermodynamic data for minerals in the system Na_2O-K_2O-CaO-MgO-FeO-Fe_2O_3-Al_2O_3-SiO_2-TiO_2-H_2O-CO_2. J. Petrol. 29, 445–522.

BEVINS, R.E. (1978): Pumpellyite-bearing basic igneous rocks from the Lower Ordovician of North Pembrokeshire, Wales. Mineral. Mag. 42, 81–83.

BEVINS, R.E., and MERRIMAN, R.J. (1988): Compositional controls on coexisting prehnite-actinolite and prehnite-pumpellyite facies assemblages in the Tal y Fan metabasite intrusion, North Wales: Implications for Caledonian metamorphic field gradients. J. Metamorphic Geol. 6, 17–39.

BIRD, D.K., CHO, M., JANIK, C., LIOU, J.G. and CARUSO, L.J. (1988): Compositional order/disorder, and stable isotope characteristics of Al-Fe-epidote, state 2-14 drill hole, Salton Sea geothermal system. J. Geophys. Res. 93, 13135–13144.

BRÖCKER, M. and DAY, H.W. (1995): Low-grade blueschist facies metamorphism of metagreywackes, Franciscan Complex, northern California. J. Metamorphic Geol. 13, 61–78.

CHO, M., LIOU, J.G. and MARUYAMA, S. (1986): Transition from the Zeolite to Prehnite-Pumpellyite Facies in the Karmuten Metabasites, Vancouver Island British Colombia. J. Petrol. 27, 467–494.

CHO, M. (1991): Zeolite to prehnite-pumpellyite facies metamorphism in the Toa Baja drill Hole, Puerto Rico. Geophys. Res. Lett. 18, 525–528.

COOMBS, D.S., NAKAMURA, Y. and VUAGNAT, M. (1976): Pumpellyite-actinolite facies schists of the Taveyanne formation near Loèche, Valais, Switzerland. J. Petrol. 17, 440–471.

CORTESOGNO, L., LUCHETTI, G. and SPADEA, P. (1984): Pumpellyite in low-grade metamorphic rocks from Ligurian and Lucanian Apennines, Maritime Alps and Calabria (Italy). Contrib. Mineral.Petrol. 85, 14–24.

DE CAPITANI, C. and BROWN, T.H. (1987): The computation of chemical equilibrium in complex systems containing non-ideal solutions. Geochim. Cosmochim. Acta 51, 2639–2652.

DE CAPITANI, C. (1994): Gleichgewichtsphasendiagramme: Theorie und Software. Beihefte zum European Journal of Mineralogy, 72. Jahrestagung der Deutschen Mineralogischen Gesellschaft 6, p. 48.

DROOP, G.T.R. (1987): A general equation for estimating Fe^{3+} concentrations in ferromagnesian silicates and oxides from microprobe analyses, using stoichiometric criteria. Mineral. Mag. 51, 431–435.

EISSEN, J.P., CRAWFORD, A.J., COTTON, J., MEFFRE, S., BELLON, H. and DELAUNE, M. (1998): Geochemistry and tectonic significance of basalts in the Poya Terrane, New Caledonia. Tectonophysics 284, 203–219.

EL-SHAZLY, A.K. and LIOU, J.G. (1991): Glaucophane chloritoid bearing assemblages from NE Oman: Petrologic significance and a petrogenetic grid for high P/T metapelites. Contrib. Mineral. Petrol. 107, 180–201.

ESPIRAT, J.J. and MILLON, R. (1965): Carte géologique de la Nouvelle-Calédonie à l'échelle du 1/50000: Feuille PAM-Ouégoa. BRGM.

EVANS, B.W. (1990): Phase relations of epidote-blueschists. Lithos 25, 3–23.

EVARTS, R.C. and SCHIFFMAN, P. (1983): Submarine hydrothermal metamorphism of the Del Puerto ophiolite, California. Am. J. Sci. 278, 1025–1056.

FREY, M., DE CAPITANI, C. and LIOU, J.G. (1991): A new petrogenetic grid for low-grade metabasites. J. Metamorphic Geol. 9, 497–509.

GAINA, C., MULLER, D.R., ROYER, J.-Y., STOCK, J., HARDEBECK J. and SYMONDS, P. (1998): The tectonic history of the Tasman Sea: a puzzle with 13 pieces. J. Geophys. Res. 103, 12413–12433.

HASHIMOTO, M. (1966): On the prehnite-pumpellyite metagraywacke facies. Geological Society of Japan Journal 72, 253–265.

HOLLAND, T.J.B. and POWELL, R. (1990): An enlarged and updated internally consistent thermodynamic dataset with uncertainties and correlations: the system K_2O-Na_2O-CaO-MgO-MnO-FeO-Fe_2O_3-Al_2O_3-TiO_2-SiO_2-C-H_2-O_2. J. Metamorphic Geol. 8, 89–124.

ISHIZUKA, H. (1991): Pumpellyite from zeolite facies metabasites of the Horokanai ophiolite in the Kamuikotan zone, Hokkaido, Japan. Contrib. Mineral. Petrol. 107, 1–7.

KRETZ, R. (1983): Symbols for rock-forming minerals. Am. Mineral. 68, 277–279.

LEAKE, B.L., WOOLLEY, A.R., ARPS, C.E.S., BIRCH, W.D., GILBERT, M.C., GRICE, J.D., HAWTHORNE, F.C., KATO, A., KISCH, H.J., KRIVOVICHEV, V.G., LINTHOUT, K., LAIRD, J., MANDARINO, J.A., MARESCH, W.V., NICKEL, E.H., ROCK, N.M.S., SCHUMACHER, J.C., SMITH, D.C., STEPHENSON, N.C.N., UNGARETTI, L., WHITTAKER, J.W. and YOUZHI, G., (1997): Nomenclature of amphiboles: Report of the subcommittee on amphiboles of the International Mineralogical Association, Commission on News Minerals and Mineral Names. Am. Mineral 82, 1019–1037.

LIOU, J.G. (1973): Synthesis and stability relations of epidote $Ca_2Al_2FeSi_8O_{12}(OH)$. J. Petrol. 14, 318–413.

LIOU, J.G. (1979): Zeolite facies metamorphism of basaltic rocks from the East Taiwan Ophiolite. Am. Mineral. 64, 1–14.

PARIS, J.P. (1981): Géologie de la Nouvelle-Calédonie, un essai de synthèse. BRGM, 240 pp.

PASSAGLIA, E. and GOTTARDI, G. (1973): Crystal chemistry and nomenclature of pumpellyites and julgoldites. Can. Mineral. 12, 219–233.

POTEL, S. (2001): Very low-grade metamorphism of northern New Caledonia. PhD thesis, Basel, 207 pp.

SCHIFFMAN, O. and LIOU, J.G. (1980): Synthesis and stability relations of Mg-Al pumpellyite, $Ca_4Al_5MgSi_6O_{21}(OH)_7$. J. Petrol. 21,441–474.

SCHIFFMAN, O. and LIOU, J.G. (1983): Synthesis of Fe-pumpellyite and its stability relations with epidote. J. Metamorphic Geol. 1, 91–101.

SCHMIDT, D., SCHMIDT, S.Th, MULLIS, J., FERREIRO MÄHLMANN, R. and FREY, M. (1997): Very low grade metamorphism of the Tavayanne formation of western Switzerland. Contrib. Mineral. Petrol. 129, 385–403.

SPRINGER, R.K., DAY, H.W. and BEIERSDORFER, R.E. (1992): Prehnite-pumpellyite to greenschist facies transition, Smartville Complex, near Auburn, California. J. Metamorphic Geol. 10, 147–170.

TERABAYSHI, M. (1988): Actinolite-forming reactions at low pressure and the role of Fe^{2+}-Mg substitution. Contrib. Mineral. Petrol. 100, 268–280.

Manuscript received December 7, 2002; revision accepted June 28, 2002.
Editorial handling: M. Engi